Landslides
DOI 10.1007/s10346-021-01651-3
Received: 18 June 2020
Accepted: 24 February 2021

Davide Notti · Aleksandra Wrzesniak · Niccolò Dematteis · Piernicola Lollino · Nunzio Luciano Fazio · Francesco Zucca · Daniele Giordan

A multidisciplinary investigation of deep-seated landslide reactivation triggered by an extreme rainfall event: a case study of the Monesi di Mendatica landslide, Ligurian Alps

Abstract In November 2016, an extreme rainfall event affected the Ligurian Alps (NW Italy). Consequently, several landslides and debris flows occurred in the upper Tanarello stream basin. In particular, the village of Monesi di Mendatica was severely damaged by two landslide phenomena: the activation of a rotational landslide, which caused the total collapse of two buildings and part of the main road, and the reactivation of a deep-seated planar massive and a complex landslide, which widely fractured most of the buildings in the village. The latter phenomenon was mostly unknown and had never been monitored prior to the 2016 event. Due to the extensive damage, the village of Monesi was completely evacuated, and the road connecting a ski resort area in the upper part of the valley was closed. Furthermore, a potentially dangerous situation related to the eventual progressive evolution of this landslide that could cause a temporary occlusion of the Tanarello stream still remains. For this reason, we defined the landslide behaviour, triggering conditions and chronological evolution leading to the 2016 event using a multidisciplinary approach. This approach consisted of field surveys, satellite DInSAR time series analyses, digital image correlation techniques, rainfall records analyses, postevent monitoring campaigns and subsurface investigation data analyses, and numerical modelling. This multidisciplinary approach enhanced our understanding of this landslide, which is fundamental to better comprehend its behaviour and possible evolution.

Keywords Extreme rainfall · Digital image correlation · DInSAR · Numerical modelling · Landslide reactivation · Multidisciplinary approach

Introduction

Worldwide, there are many landslides that have the potential to reactivate. However, many of them are not monitored by in situ measurement systems, and if they reactivate, the catastrophic phase cannot be directly registered. In such cases, one of the initial activities carried out during a scientific or technical investigation is the identification of the recent landslide's evolution and characterization of its kinematics. These goals can be achieved by using a multidisciplinary approach that combines traditional and innovative elements, such as remote sensing data, meteorological data, field surveys and numerical modelling (Mantovani et al. 2013; Peduto et al. 2018; Tomás et al. 2018).

It is well known that some of the primary triggers of landslide reactivation are extreme rainfall events. Many studies focus on the definition of critical rainfall thresholds for landslide activation (Iverson 2000; Peruccacci et al. 2017). In general, rainfall thresholds perform better for shallow landslides or debris flows (Guzzetti et al. 2008; Tiranti and Rabuffetti 2010) than for deep-seated landslides (Zêzere et al. 2005; Guzzetti et al. 2007; Gao et al. 2018). The latter are more sensitive to long-term conditions, complex combinations of geomechanical parameters and various landslide geometries, so the corresponding rainfall thresholds are more difficult to determine. Several examples of massive and large landslide reactivations due to extreme rainfall events have been reported in the literature. Focusing on European cases, we note the Val Pola rock avalanche in the central Alps in 1987 (Crosta et al. 2004), the Corniglio landslide in the Northern Apennines in 1994 (Bertolini and Pizziolo 2008), the Alpe Baranca DSGS in the NW Alps in 2000 (Ramasco and Troisi 2002), the Mount Gírová landslide in the West Carpathian in 2010 (Baroň et al. 2011) and the Stogovce landslide in the Slovenian Alps in 2010 (Petkovšek et al. 2011).

According to the Intergovernmental Panel on Climate Change (IPCC), one of the consequences of global warming is an increase in extreme rainfall events over certain areas (IPCC 2014). Such an increase in extreme events could be favourable for landslide activation (Crozier 2010; Stoffel et al. 2014; Gariano and Guzzetti 2016; Handwerger et al. 2019).

In recent years, the Ligurian Alps (the southwestern extremity of the Italian Alps) has been affected by severe rainfall events during the autumn season. These events ranged from concentrated flash floods that mainly triggered shallow landslides, such as that in 2011 (Avanzi et al. 2015) or 2014 (Amanti et al. 2016; Giordan et al. 2017a; Cignetti et al. 2019), to persistent rainfall over vast areas that triggered deep-seated landslides, such as during the floods that occurred in 1994 (Luino 1999) and 2000 (Guzzetti et al. 2004). In some of these cases, the extreme events reactivated landslides that were not monitored. Consequently, the reconstruction of landslide kinematics cannot be performed based on in situ measurement data acquired during the events. Instead, a composite strategy based on postevent monitoring, numerical modelling and field survey data should be adopted.

Remote sensing offers great support in studying landslides when in situ monitoring and ancillary data are missing. In particular, it provides an excellent tool to reconstruct landslide kinematics during its rapid phase. In recent years, among the various remote sensing techniques, further support has been provided by digital image correlation (DIC). DIC is an image analysis technique that has been widely applied to aerospace optical or SAR images to measure the surface deformation associated with landslides (Stumpf et al. 2017; Bickel et al. 2018; Caporossi et al. 2018; Manconi et al. 2018), glaciers (Scambos et al. 1992; Debella-Gilo and Kääb 2011; Giordan et al. 2020) and other geomorphological processes (Leprince et al. 2007). Another significant contribution

Published online: 21 March 2021

has come from InSAR satellite data, which are currently one of the most commonly used sources for slow landslide monitoring (Casagli et al. 2016; Béjar-Pizarro et al. 2017; Frattini et al. 2018).

Another helpful approach in investigating landslides, with unknown pre-failure conditions due to their unexpected reactivation, is the back-analysis method based on numerical modelling. It can be used to estimate slope conditions at the time of failure in terms of strength parameters and pore water pressure. Back analysis, in the absence of direct monitoring data, can be considered an effective method to provide insight into the underlying failure mechanisms of landslides and improve knowledge on landslide kinematics and the factors controlling its stability (Crosta et al. 2004; Lollino et al. 2014, 2016; Longoni et al. 2016; Berti et al. 2017; Cevasco et al. 2018; Agliardi et al. 2020).

In this study, we analyse the activation of two landslides that occurred in the village of Monesi di Mendatica in the Ligurian Alps after an extreme rainfall event in November 2016. In particular, during this event, the village was partly destroyed by the activation of a rotational landslide that caused the collapse of two buildings and the main road (hereafter L1) and the reactivation of massive and deep-seated planar landslide that damaged most of the buildings (hereafter L2). The activation of the main landslide L2 poses a potential danger because further movement of this large mass could cause the temporary closure of the Tanarello stream. As this landslide was not monitored by an in situ monitoring system and as it was largely unknown until the 2016 reactivation, we used a multidisciplinary approach to study its kinematics and correlations with meteorological data. To characterize the Monesi landslide, we divided our multidisciplinary work into the following steps:

(i) We investigated past landslide activity and geomorphological evidence; (ii) we reconstructed the evolution of the catastrophic phase and its correlation with rainfall; (iii) we mapped and analysed the geomorphological effects and structural damage based on field surveys; (iv) we analysed remote sensing data, i.e. we used the DInSAR time series to define the movement before and after the main event; (v) we applied the digital image correlation (DIC) technique to the satellite and high-resolution aerial photo images to estimate the coevent displacement magnitude and distribution; (vi) we analysed postevent monitoring and subsurface investigation data to estimate the geotechnical parameters, groundwater behaviour and landslide depth; and (vii) we numerically modelled the slope behaviour during the 2016 precatastrophic phase by means of the finite element method (FEM), which was aimed at estimating both the critical groundwater level that dropped the slope safety factor to unity and the shear strain localization within the landslide body. Additionally, we studied the effect of the failure of rotational landslide L1, which was located at the toe of the L2 landslide, on the stability of the entire slope by performing numerical analyses on the reprofiled slope geometry.

Study area

The present study area is located in the upper part of the Tanarello Valley (a tributary of Tanaro river), in the Ligurian Alps, on the border between the Liguria and Piemonte regions (NW Italy). The basin has a surface area of approximately 11 km^2, and the elevation ranges from 2200 m a.s.l. at M. Saccarello to 1100 m a.s.l. in the Tanarello streambed. There are three small villages in the valley: Piaggia (Piemonte region), located on the north side of the valley, and Monesi di Triora and Monesi di Mendatica (Liguria region), which are located on its south side. All villages were affected by the November 2016 extreme rainfall events, and in particular, Monesi di Mendatica was severely damaged and partially destroyed by the two landslides (Fig. 1).

Geological settings

The area is located in the San Remo-Monte Saccarello Formation, which is a part of the Cretaceous-Paleocene Helminthoid Flysch, a complex of the Penninic Nappe of the Western Ligurian Alps (Vanossi et al. 1984). The Helminthoid Flysch overthrusts the formations of the Helvetic structural domain south of M. Frontè (Maino and Seno 2016). The Bordighera sandstone formation, also as a part of the Helminthoid Flysch, crops out NE of the study area. In this sector, the Saccarello Flysch is composed of an alternating sequence of thick layers of calcareous sandstone and marl and thin layers of siltstone or shale (Pepe et al. 2015). According to the GSI rock mass classification (Marinos and Hoek 2000), this portion of the San Remo Formation is classified as good (GSI = 45) (Pepe et al. 2015). The bedding of this formation trends from N-NW to NE with a dip of approximately 20°–30°. Such a structural setting favours slope instability on the south side of the Bavera-Tanarello valley.

According to a geological map of France (Lanteaume et al. 1990), several quaternary deposits on the south side of the valley have been detected (Fig. 1). These deposits are mainly composed of landslide bodies, taluses and some glacial deposits from the last glaciation. In this area, landslide bodies are usually derived from the degradation of flysch formations, this exposing their predominant block-in-matrix nature, as is typical of landslides affecting this lithology (Berti et al. 2017).

Geomorphological settings

The upper valley of the Tanarello-Bavera streams is oriented SW-NE. The structural setting influences the morphology of the valley. The north flank of the valley is characterized by a steep slope oriented to the SSE with an anti-dip setting. On this side, near the village of Piaggia, it is possible to observe a terraced landscape that is mostly abandoned. The south side of the valley presents a gentler dip slope, and it is possible to detect several landslide bodies already mapped in IFFI (*Inventario dei fenomeni franosi in Italia,* in Italian), which is the Italian landslide database (Trigila et al. 2008). During the extreme rainfall event that occurred in autumn of 2000, landslide reactivation caused moderate damage to some buildings in the resort village of Monesi di Triora (Federici et al. 2007). The 2016 event caused a major reactivation of the Monesi di Mendatica landslides (L1 and L2 in Fig. 1).

According to the IFFI, the village of Monesi di Mendatica is located in the lower sector of a complex massive inactive landslide, which was reclassified as active after the 2016 event (L2 in Fig. 1). This sector of the landslide presents a wedge-fan shape. A landslide deposit caused the deviation of the Tanarello stream from the valley axis, likely during the Holocene epoch. The landslide toe is characterized by a steep slope related to the still active erosion process of the Tanarello stream. It is interesting to note the path of the small Bandita Creek that currently crosses the landslide

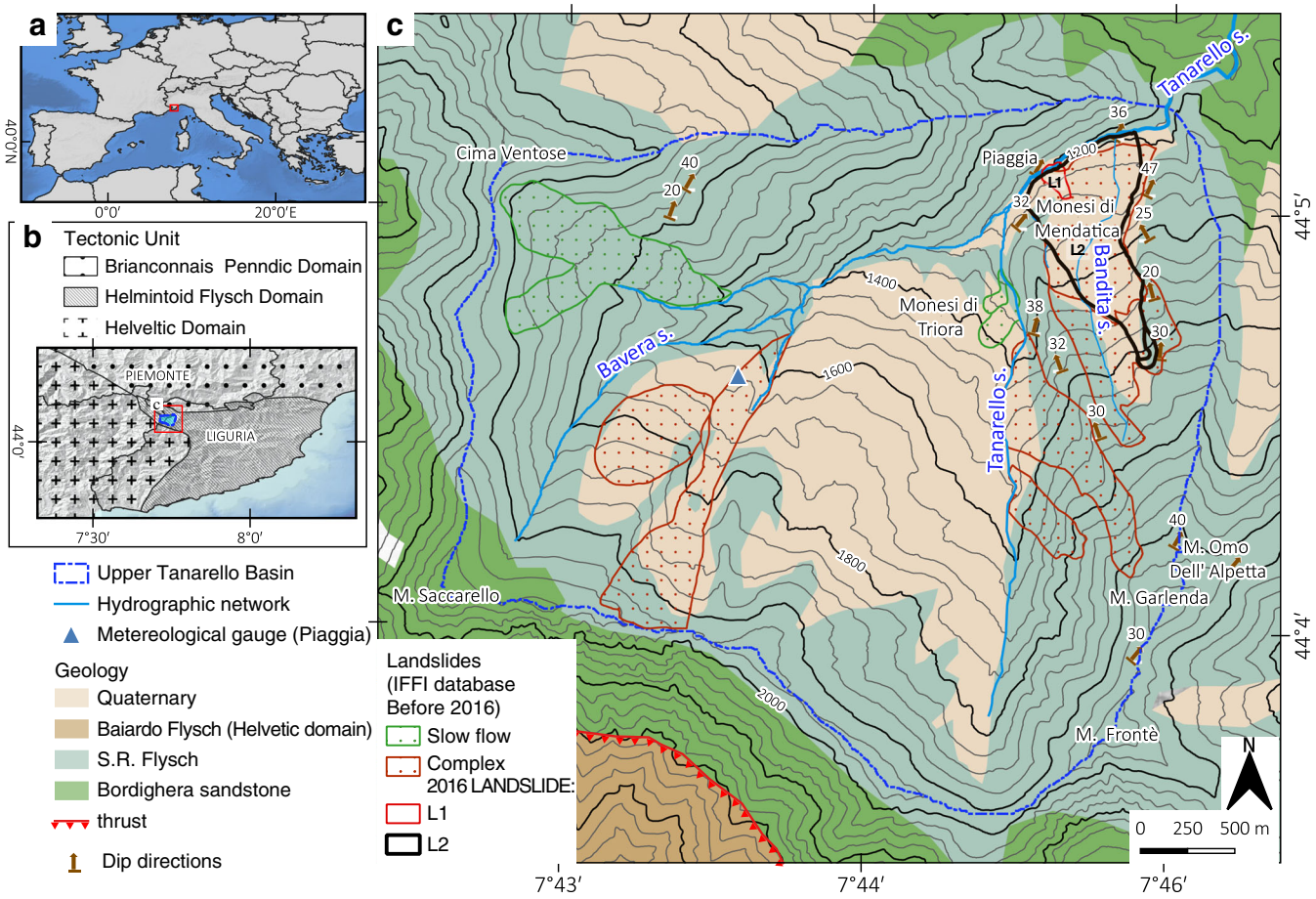

Fig. 1 **a** Location of the study area, **b** structural settings of the Ligurian Alps and **c** geological framework of the upper Tanarello catchment modified from Lanteaume et al. (1990) with overprinted landslides identified in the IFFI inventory and with landslides that occurred in Monesi di Mendatica during the 2016 event

deposit. Its original flow direction likely deviated after ancient landslide activity. During the 2016 extreme rainfall event, Bandita Creek likely contributed to an increase in the water load on the landslide.

Materials and methods

In the present work, to characterize the evolution of the Monesi landslide (i.e. before, during and after the 2016 event), we used various data types (meteorological data, remote sensing data, postevent ground-based monitoring surveys and subsurface investigation data, technical reports and other publicly available data) and processing methodologies (manual analyses, DIC technique and numerical modelling). In the following, we present their detailed descriptions.

Rainfall and hydrological data for the 2016 event and historical data comparison

Daily rainfall data from 1957 to 1999 were extracted from the meteorological grid dataset of the Piemonte region. The rainfall data were interpolated using a NWIOI (northwestern Italy optimal interpolation) grid (Turco et al. 2013) with a 0.125° spatial resolution. This dataset is available at no cost on the ARPA Piemonte website (ARPA Piemonte 2017).

Daily rainfall datasets recorded since 1999 by the Piaggia gauge (located approximately 2 km west of the Monesi landslide) are available in the ARPA Piemonte database. Additionally, meteorological data from the old Piaggia gauge (1945–1991) are available in the Hydrological Yearbooks archive of the ISPRA (ISPRA 2012). In this archive, the maximum cumulative rainfall over a 5-day interval for each year is reported. These data are likely in agreement with the rainfall extracted from the ARPA Piemonte dataset. From the gathered rainfall data, we selected the most extreme rainfall events that occurred in the area of Monesi over the past 75 years.

For the 2016 event, to obtain a precise temporal correlation between the rainfall and the sequence of events, we used hourly and cumulative rainfall datasets from ARPA Piemonte and Regione Liguria rain gauge stations near Monesi (Table 1). We chose the nearest station (Piaggia) as a reference for comparison. Piaggia is the small village located on the opposite side of the valley with respect to Monesi. Additionally, we collected hourly level data for the Tanarello stream (estimated from the Ponte di Nava gauge, 10 km downstream from Monesi).

Table 1 Meteorological stations close to Monesi Landslide

Name	Basin	Source	Parameters	Elevation (m)	Distance (km)	Directions
Piaggia	Tanarello	ARPA Piemonte	Hourly/daily rainfall	1645	2.0	WSW
Piaggia	Tanarello	ISPRA	Historical data	1310	0.5	NW
Verdeggia	Argentina	Regione Liguria	Hourly rainfall	1120	4.7	S
Poggio Faerza	Arroscia	Regione Liguria	Hourly rainfall	1845	5.0	SE
Upega	Negrone	Arpa Piemonte	Hourly rainfall	1310	6.1	NW
Pornassio	Arroscia	Regione Liguria	Hourly rainfall	475	9.2	E
Ponte di Nava	Tanaro	Arpa Piemonte	Hourly rainfall/river level	840	10.1	NE
Pieve di Teco	Arroscia	Regione Liguria	Hourly rainfall	263	13.2	E

We decided to use the discharge rate and Tanarello stream level to assess the role of foot erosion during the first phase of L1 and L2 reactivation.

Remote sensing optical data: satellite and high-resolution images

In Table 2, we listed the remote sensing optical data and the corresponding processing methodologies, which we used to identify landslide limits and obtain coevent displacements. We applied the DIC technique to the images of the Sentinel-2 and Planet satellites to calculate the coevent displacements. We used Google Earth, LiDAR, aerial and Pleaides images to manually measure the displacement and for landslide mapping. In the following, we describe the processing of the presented datasets.

Digital image correlation for coevent displacement estimation

DIC is an image analysis technique that searches for patches in master and slave images that maximize a given similarity function (Fienup 1997). Therefore, DIC provides spatially distributed maps of the two displacement components that are orthogonal to the line of sight (LOS). One of the most commonly used similarity functions is the zero-mean normalized cross-correlation (Dematteis and Giordan 2021), which is calculated considering a reference template out of the master image and is searched for in a larger investigated area of the slave image. The ZNCC is calculated for every template candidate of the investigated area, obtaining the ZNCC surface. We adopted an interpolation function in the neighbourhood of the ZNCC peak to achieve subpixel sensitivity. We applied the DIC technique to the Sentinel-2 and Planet Scope images (pre- and postevent images).

In this study, we adopted a five-step DIC procedure:

1. Image selection: We used images acquired within the same period of the year and at similar hours to guarantee a similar sun elevation and azimuth to minimize shadow changes that might introduce ZNCC artefacts (Dematteis et al. 2019). Moreover, we discarded images with snow coverage or clouds, especially those nearby the landslide areas; we also discarded images with different orthorectifications. These filters limited the number of suitable satellite images, but they increased the probability of having more accurate results.
2. Monochromatic conversion: We converted the RGB optical photographs into monochromatic images.
3. Co-registration: We co-registered the images by conducting a rigid translation according to the pixel offsets computed within a reference area that was assumed to be stable.
4. Displacement calculation: We calculated the ZNCC in a window that slid onto a regular grid that covered the whole image. Template overlap allowed an increase in the spatial resolution of the maps.
5. Outlier identification: We refined the results by adopting statistical local metrics to identify and discard outliers (Dematteis et al. 2018).>

Manual measure of displacement and landslide mapping based on high-resolution images

We performed manual measurements of the displacement by comparing high-resolution images, i.e. postevent LIDAR and UAV images (2017), with pre-event orthophotographs of Regione Liguria (2015). Additionally, we estimated the displacement magnitude based on Google Earth images available for the study area at a high spatial resolution (≈ 0.25 m/pixel) for both pre- and post-2016 events. In particular, we calculated the horizontal movement of the centroids for some well-defined ground targets (e.g. rock and buildings). To assess the overall effects of the 2016 event, we also manually mapped all the landslides in the upper Tanarello catchment using Google Earth, Pleiades and Sentinel-2 images.

Estimation of pre- and postevent velocities based on InSAR data

In Table 3, we present the InSAR dataset from the Radarsat and Sentinel-1 satellites along with their main characteristics, which we used to obtain pre- and postevent landslide velocities.

The InSAR data, provided by Regione Liguria, cover the periods of 2003–2009 (Radarsat satellite) and 2014–2019 (Sentinel-1 A/B). These data were processed with the SqueeSAR™ algorithm (Ferretti et al. 2011). Ascending and descending geometries are available for both satellites. Concerning the earlier periods, the dataset covering the period of 1995–2000 (ERS satellite) is available on the Not-Ordinary Plan of Remote Sensing (PST) of the Italian Ministry of the Environment. However, due to their low density, we did not consider them in this study.

A positive V_{LOS} value indicates movement towards the satellite, while a negative V_{LOS} value indicates movement in the opposite direction. To compare the measurements of the ground-based

Table 2 List of aerial and satellite data used to map landslides and extract the coevent displacement

Sensors	Spatial resolution (m)	Pre-event image date	Postevent image date	Methodology	Product obtained
Sentinel-2	10	29/09/2016	29/09/2018	DIC	2D displacement
Planet (Planetscope)	2/3	03/10/2016	06/10/2017	DIC	2D displacement
Google Earth	0.3	24/09/2015	03/08/2017	Manual interpretation	2D displacement and mapping
LIDAR/Aerial Photo	0.2	2015	2017	Manual interpretation	2D displacement and mapping
Pleiades	0.5	2015	2017	Manual interpretation	Mapping

systems with the InSAR measurements, we represented the velocity along the LOS (V_{LOS}) as the velocity along the slope orientation (V_{SLOPE}). V_{SLOPE} is calculated as the ratio between the V_{LOS} and the percentage of movement detected along the LOS (C) (see Eq. 1) (Notti et al. 2014; Béjar-Pizarro et al. 2017). Reciprocally, we projected the displacement measured by other instruments along the LOS to compare the time series using the same Eq. 1.

$$V_{SLOPE} = (V_{LOS}/C) \quad (1)$$

We inverted the sign of the resulting V_{SLOPE} to be compatible with the rest of the results. We used the Radarsat datasets only for analysing the velocity, while Sentinel-1 data, which have a better quality, were also used to analyse the displacement time series.

Postevent ground-based data

Subsurface investigations

In the period between 2017 and 2019, several subsurface investigations were performed to define the geological, geotechnical and hydraulic properties of the landslide mass. The drilling campaign included ten boreholes located in the area of Monesi di Mendatica (see Fig. 2c′). The drilling depths of each borehole are as follows: 48 m (borehole S1), 60 m (borehole S2), 62 m (borehole S3), 24 m (borehole S4), 55 m (borehole S5), 12 m (borehole S6), 12 m (borehole S7), 42 m (borehole S8) and 47.5 m (borehole S9 and S9b). The S6 and S7 boreholes were drilled outside the landslide deposits to support the design of the new road system to bypass the most active part of the landslide and reconnect the upper part of the valley and the ski resort area. The reached borehole depths allowed us to define the landslide thickness and quality of the bedrock, as well as to anchor the inclinometric tubes. The reported bedrock quality was variable. The RQD index was determined to be good (RQD > 75%) for boreholes S1 and S3, while for the other cases, it was classified as poor (RQD < 50%) (Pepe et al. 2015). The drilling results highlighted the presence of large (exceeding the unit volume) calcareous boulders within the landslide deposit.

Ten SPTs (standard penetration tests) were attempted during borehole drilling: two per borehole in S1, S2, S3, S4 and S5. However, the presence of large blocks and the heterogeneous nature of the deposit resulted, in many cases, in an excessive number of blows at various depths, so the corresponding results were not useful. The only successful attempts were performed for boreholes S2 (at a depth of 1.50 m with 7-8-20 blows), S3 (at a depth of 10.50 m with 6-10-8 blows) and S4 (at a depth of 12 m with 17-23-21 blows). Additionally, four Lefranc permeability tests were performed at different depths in boreholes S1 (27–28 m), S3 (33–34 m), S4 (16.6–17.6 m) and S5 (6.5–7.5 m), and the reported permeability coefficients were 3.18 10^{-6}, 4.5 10^{-6}, 2.11 10^{-4} and 1.83 10^{-4} m/s. Finally, one seismic campaign based on the MASW (multichannel analysis of surface waves) methodology was conducted, allowing for the seismic exploration and evaluation of subsoil stiffness. For this purpose, five stations with 12 geophones each were installed just above the village (see Fig. 2c′). Each investigation indicated the predominant block-in-matrix nature of the L2 landslide.

Postevent monitoring instruments

After the 2016 event, the authorities (ARPA Piemonte, Municipality of Mendatica and Regione Liguria) decided to monitor the slope. This landslide is potentially dangerous because further evolution could temporarily block the Tanarello steam. Several monitoring techniques were adopted to monitor its superficial and deep-seated displacement and crack extension and the resultant groundwater conditions. In particular, two piezometers, four inclinometers, nine topographic prisms, with total station positioned on the opposite flank of the valley, twenty-two crack metres and nine GNSS benchmarks were installed within the landslide body, on the buildings in the village of Monesi, and in the nearby stable areas (see supplementary material for the location of

Table 3 List of InSAR satellite data used to map pre- and postevent displacements

Satellite	Geometries available	Temporal span	Processing methodology	Available products	Post-processing analysis
Radarsat	Ascending and descending	2003–2009	SqueeSAR™	V_{LOS} Time series	V_{SLOPE}
Sentinel-1 A/B	Ascending and descending	2014–2019	SqueeSAR™	V_{LOS} Time series	V_{SLOPE}, Time series analysis

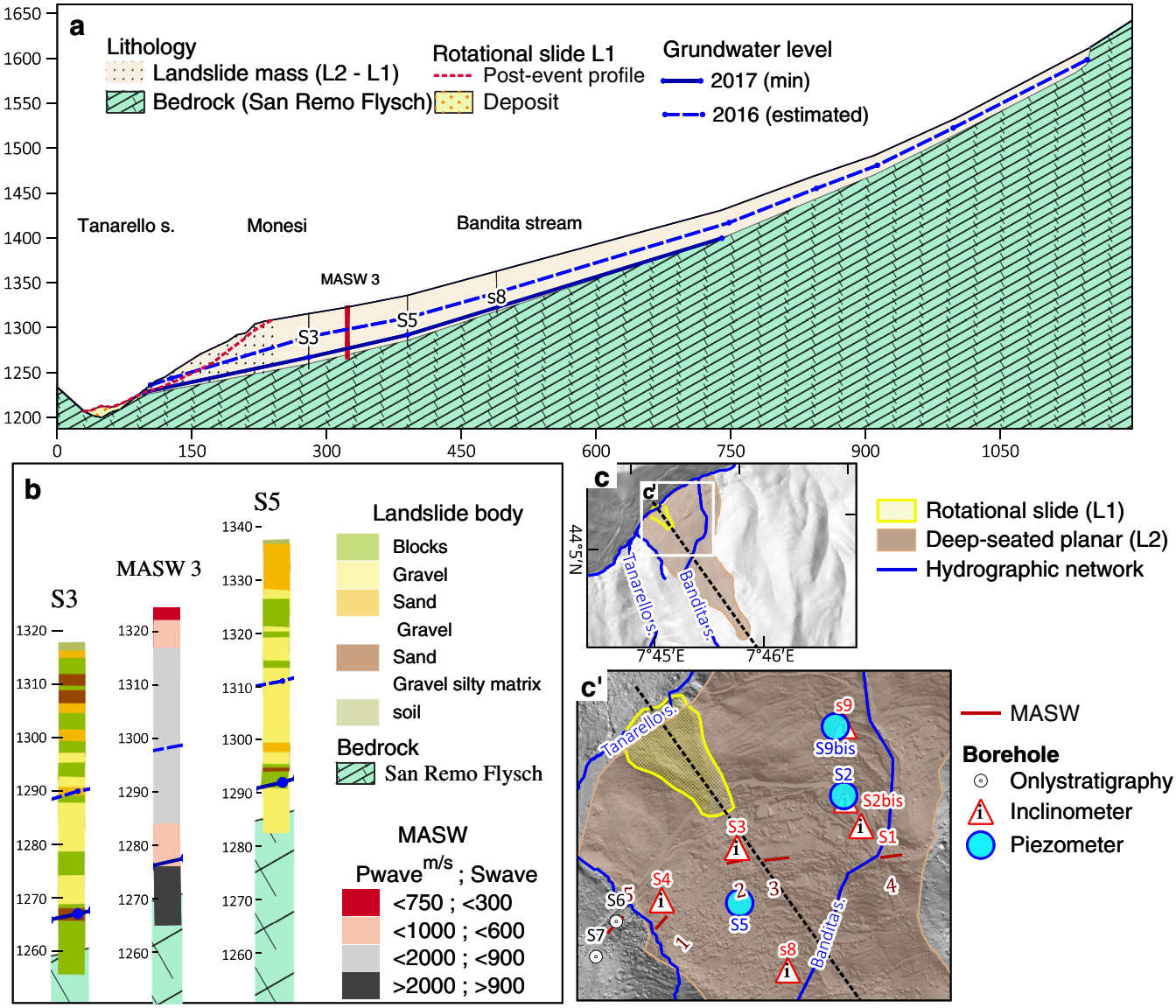

Fig. 2 a Lithological profile and groundwater level. b Details of borehole stratigraphy and MASW near cross-section. c Location of the profile. c′ Borehole and MASW investigations

monitoring instruments). Table 4 summarises the monitoring instruments installed after the 2016 event with the measurement frequencies and acquisition spans considered in this study.

Unfortunately, we could use only a subset of these measurements (Table 4), as some of them were not suitable for our study because they either provided unreliable data or did not provide information regarding landslide movement. In particular, the inclinometric measurements, likely due to technical issues during the inclinometric tube installation, were not reliable. Only one inclinometer provided acceptable data to be considered in the postevent analysis. We also did not consider crack metre data, as they did not directly provide any information about landslide movement.

We used piezometric data to interpret the groundwater level response to precipitation, and we analysed the surface displacement measurements (topography and GNSS) to estimate the postevent residual movement. Additionally, the postevent monitoring data provided some indications for numerical modelling, e.g. hydraulic conditions and sliding surface depth (§ Numerical modelling: Setup of the landslide model).

Ancillary data, photographs and field survey

Until the 2016 event, the Monesi deep-seated planar landslide (L2) was not the subject of many investigations. The documents collected prior to the event consisted of the following:

1. The SCAI (Italian atlas of towns affected by slope instabilities) technical report (Federici et al. 2007), which was limited to effects on the village and provincial roads;
2. The IFFI database;

Table 4 Monitoring instruments installed after the 2016 event

Instrument	Number of instrument	Temporal span	Measurements frequency	Used for this work
GNSS benchmarks	9	June 2017–June 2019	2/3 per year	Yes
Topographic prism	9	April 2017–May 2019	2 per year	Yes
Piezometers	2	October 2017–November 2019	4 per day	Yes
Inclinometers	4	October 2017–December 2019	2 per year	Partly (only for the depth of movement)
Crack metres	20	April 2017–May 2019	2 per year	No

3. Aerial photographs analysis, which was used to detect the pre-event morphology of the landslide; this type of analysis is also available in the ARPA Piemonte technical report (ARPA Piemonte and Regione Piemonte 2018);
4. Newspapers and other historical sources, which were analysed in search of information on ancient damage related to landslides.>

To reproduce the evolution of the landslide catastrophic phase, we analysed photographs and descriptions of the partial events from technical reports issued by the ARPA Piemonte (ARPA Piemonte and Regione Piemonte 2018) and from web news. The time of landslide activation and the period in which the major displacement of the deep-seated planar landslide L2 occurred are essential to determining the right order of events.

During the postevent field survey performed in the summer of 2018, we defined the geomorphological effects and damages to the structures. We mapped the geomorphological evidence of L1 and L2 reactivation. During the field observation survey, we evaluated the damage to the buildings and other structures using a qualitative methodology described by Cooper (2008). In this approach, the damage could be defined according to seven degrees of damage ranging from no damage (degree I) to total collapse (degree VII) based on visual observations taken in the field. Furthermore, we used high-resolution UAV and LIDAR DTM images to improve detection and mapping of geomorphological elements. During field surveying, we also annotated signs of possible ancient landslide reactivation, such as curved trees.

Numerical modelling: setup of the landslide model

To simulate the failure mechanisms and conditions leading to the observed slope failure, a two-dimensional numerical model of the slope was developed. In the present work, we performed a finite element analysis of the entire slope aimed at assessing the stress-strain behaviour of the slope in response to variations in the groundwater level; in particular, a parametric analysis was performed to calculate the critical groundwater level corresponding to the triggering of failure conditions as well as the associated failure mechanism. For this purpose, data related to slope geometries, geotechnical and hydraulic properties of the materials, hydraulic and mechanical boundary conditions, initial stress state of the slope, and constitutive behaviour of the soil materials were used as presented in the following sections.

Slope geometry

Based on the boreholes drilled within the lower part of the entire landslide area, we assumed that the landslide body was composed of a heterogenic mixture of materials, including large blocks of limestone, heterometric breccia and gravel within a soil matrix ranging from sandy-silty to clayey-sandy. The landslide body was likely generated by the disintegration of the bedrock. Additionally, the results from the MASW showed a quasi-homogeneous wave distribution, so there was no evidence of single layers and/or shear bands. Therefore, we assumed that the slope was composed of two domains: the bedrock and landslide body. The slide mass thickness varies from 10 to 60 m, and its length is approximately 1100 m. The landslide topography was simplified from the DTMs of 2006 (pre-failure geometry) and 2017 (post-failure geometry). Finally, the longitudinal cross-section was described along the maximum slope direction (Fig. 2a).

Hydraulic conditions and parameters

The detailed groundwater conditions at the time of failure are unknown. The only available indication prior to the failure event was the presence of a water spring at the landslide toe, at an elevation of approximately 1250 a.s.l., which was considered the outflow point of the groundwater level during the critical conditions. Based on the available postevent piezometer data from 2017 to 2019, we assumed that the unconfined aquifer within the landslide mass was characterized by a water table (defined in piezometer 5) varying from 43 to 25 m below ground level. The latter value was supposed to correspond to the failure conditions and was consistent with the elevation of the water spring at the toe. The maximum groundwater level was defined based on the piezometric data analysis (§ Piezometric data and correlation with rainfall and snow melting) and field observations (§ Geomorphological mapping and damage assesment).

Additionally, the material permeability was defined by the Lefranc test. Considering the boreholes near the cross-section, the reported values were 0.39 m/day (borehole S3) and 15.81 m/day (borehole S5). For numerical modelling, the mean value was chosen (8.1 m/day) for the landslide body. Regarding the bedrock, we assumed that the material composing the bedrock was impermeable due to the presence of a high-quality low-fractured rock formation, which should have created a hydrological barrier for the infiltrating water.

Geotechnical parameters

The bedrock consists of the San Remo Flysch Formation, which is widely outcropping in Western Italy (Pepe et al. 2015). The stiffness

and strength parameters of this formation were reported in Pepe et al. (2015) in which geological strength index (GSI) values are identified and soil strength parameters are defined according to the Hoek-Brown criterion and the equivalent Mohr-Coulomb parameters (Hoek and Brown 2019). The San Remo Flysch Formation in the area of Monesi is classified as a good-quality rock mass. The parameters used for numerical modelling are listed in Table 5.

Regarding the landslide body, due to its heterometric sorting, the extraction of specimens appeared very difficult, so geotechnical characterization through laboratory testing could not be performed. Since the landslide debris is supposed to be mainly the result of destruction and remoulding of the underlying bedrock due to landslide activity, the friction angle of the landslide debris is assumed to remain approximately the same as that of the rock parent formation, while the cohesion value is supposed to be much lower than that of the bedrock as a consequence of the loss of the cementation degree of the materials forming the landslide debris. In particular, for the highest groundwater level (i.e. that corresponds to the landslide activation), a safety factor equal to SF = 1 was obtained when a cohesion equal to c = 47 kPa was set for the landslide body. Therefore, this value was assumed to be the cohesion value mobilized at failure.

The elastic parameters of the landslide mass, i.e. Young's modulus (E) and Poisson's ratio (ν), were assumed to be equal to 1.0510^{6} kN/m^2 and 0.37, respectively, based on the results obtained from the MASW measurements and according to the literature formulations (Park et al. 1999).

Landslide simulations

The two-dimensional finite element software PLAXIS (PLAXIS 2D 2019), using 15-node elements and plane-strain analysis under drained conditions, was selected to perform analyses of the slope behaviour. The adopted model discretization for pre- and postevent geometry is shown in Fig. 3a and Fig. 3b, respectively. The mesh is formed of 2324 elements and 19001 nodes (pre-event geometry) and 2270 elements and 18,550 nodes (postevent geometry). Significantly smaller element sizes were arranged for the landslide mass to increase the calculation accuracy in this domain. An isotropic elastic-perfectly plastic constitutive model, with a Mohr-Coulomb failure criterion and a non-associated flow rule, was assumed for all the materials involved. Standard displacement boundary conditions were implemented, i.e. vertical and horizontal displacements are prevented at the base of the domain and fixed horizontal displacements are imposed on the lateral boundaries. The pore water pressure distributions were calculated from prescribed phreatic levels, as described below. The initial state of stress for the slope was computed through a gravity loading procedure, i.e. gravitational loads were applied under elastic material conditions.

Later, a plastic analysis with the assigned material properties (Table 5) was carried out. This analysis was followed by a strength reduction analysis aimed at calculating the corresponding safety factor. According to this method, the safety factor was obtained by continuously decreasing the value of cohesion and friction angle of the soil until nonconvergence in the model was reached (Dawson et al. 1999). The indication of failure was detected either by monitoring the achievement of numerical convergence during the plastic analysis or, in the case of numerical convergence, by verifying the safety factor from the strength reduction analysis, which was very close to 1.0. The simulations were initially carried out with respect to the geometry of the pre-failure slope, which was composed of landslide mass and bedrock, as shown in Fig. 2a.

To investigate the influence of groundwater level variation generated by the infiltration process of the rainfall event, a parametric analysis concerning the groundwater level depths was carried out, keeping the mechanical parameters reported in Table 5 fixed. We defined seven hydraulic conditions: the GWL measured in 2017 by piezometer 5 (at approximately 43 m below ground level), the GWL estimated in 2016 during the rainfall event (at approximately 25 m below ground level) and five intermediate GWLs (at steps of approximately 3 m). We assigned the dry condition to the bedrock due to its impermeable characteristics.

Regarding the effects of L1 failure on the general stability of the entire slope, we proposed a new model in which we changed the slope geometry in accordance with this landslide occurrence. In particular, a reprofiling of the ground surface in the lowest portion of the slope consistent with the failure of the L1 landslide was reproduced (Fig. 3b). In this simulation, the mechanical properties of the slope materials were left unchanged (see Table 5), and the groundwater level was set to 25 m below ground level.

Results

Past activity of the Monesi landslide

The evidence collected from aerial photos and technical reports suggested the following:

1. According to the SCAI technical report, the Monesi di Mendetica landslide (which mostly coincides with the L2

Table 5 Parameters used for the numerical modelling

Parameters	Symbol	Units	Landslide mass	Bedrock
Young modulus	E	[kN/m^2]	$1 \cdot 10^6$	$5 \cdot 10^7$
Poisson ratio	v	[-]	0.37	0.4
Cohesion	c′	[kN/m^2]	47	2400
Friction angle	φ′	[°]	37	37
Permeability	$K_x = K_y$	[m/day]	8.1	DRY
Dry unit weight	γ_d	[kN/m^3]	20	26.5
Saturated unit weight	γ_{sat}	[kN/m^3]	23	30.5

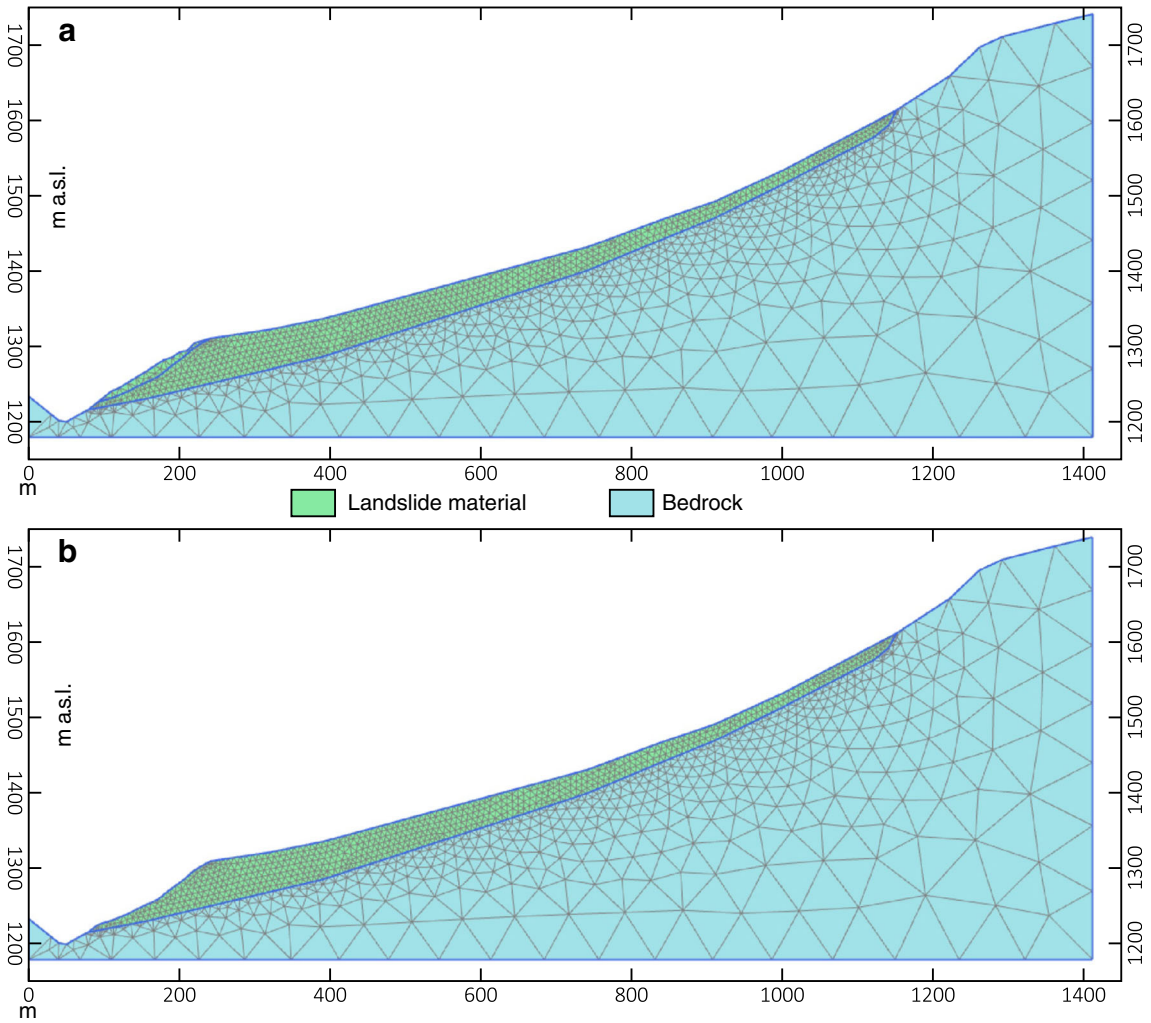

Fig. 3 Model discretization used in the numerical analyses. a Pre-event. b Postevent

landslide) has been classified as dormant (Federici et al. 2007). The authors, during field surveying, detected slight damage to some buildings and observed fractures along the provincial road (near the 2016 L1 failure), which were probably related to the 2000 and 2002 events. Some of these signs were still present in 2011, as they are visible in Google Street View images. The authors finally suggested installing a monitoring system as a precautionary measure.

2. The landslide shape, based on aerial photograph interpretation made by the ARPA Piemonte after the flood event, is better defined than the landslide shape mapped in the IFFI inventory. We note that in 2016, the reactivation affected almost the entire area of the pre-existing landslide (Fig. 4).
3. Historical photographs and postcards suggest that in the past (early 900 s), the middle-lower sector of the slope was terraced for agriculture and pasture activities, and a small village was settled there before the construction of a ski resort. Today, the terraces are mostly abandoned.
4. Geomorphological evidence, i.e. curved tree trunks in some areas, suggest that the landslide was locally affected by movements and reactivation.

Based on the gathered data, we cannot determine if and when the landslide was historically subject to massive reactivation. However, the deviation of the Tanarello stream from the central axis of the valley and its erosion at the toe of the slope suggest that the deep-seated planar L2 landslide is not a relict process. In addition, the Bandita Creek path is likely related to the evolution of the landslide and suggests periodic movement of the mass. Conversely, all the collected data indicate that the L2 landslide was not affected by severe reactivations involving the whole landslide body, at least within the last 70 years.

The area affected by the rotational landslide (L1) already experienced minor reactivations. The provincial road that crosses the landslide crown was already damaged before 2016, as observed in the Google Street View image from 2011 (photos I and II in Fig. 4).

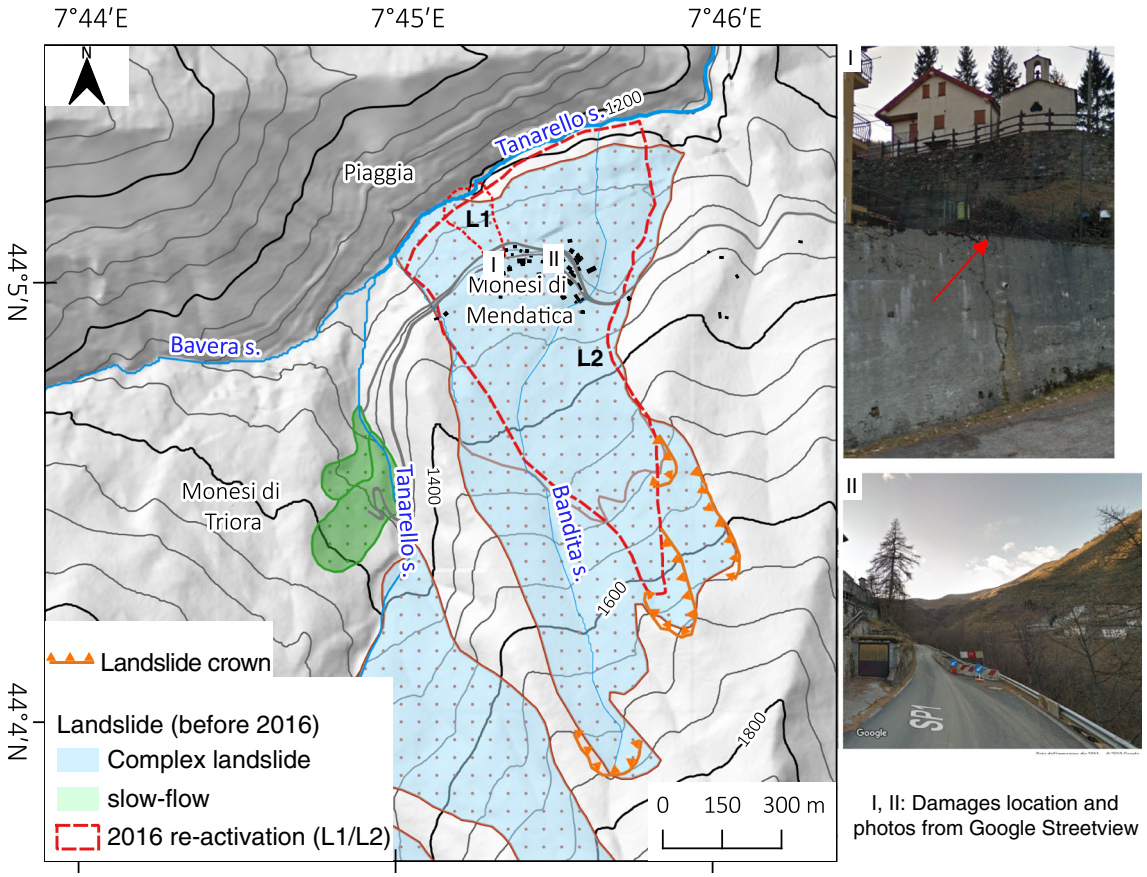

Fig. 4 Pre-2016 landslide shape from IFFI, evidence of minor damages: (I) a crack along retaining wall in 2011; and (II) a small road collapse in 2011 located in the same position of the crown of a rotational landslide L1 triggered by the 2016 event

Rainfall analysis of November 2016 compared with previous extreme events

Extreme rainfall events are known to be one of the main triggers of landslide activation. For this reason, we collected and analysed rainfall records from the past 75 years. In Fig. 5, we present a comparison of these events. Based on a historical rainfall dataset, we estimated that the November 2016 event was the most severe event that occurred with a temporal span of 5/6 days in the last 75 years. This event exceeded the other significant events by approximately 200 mm, and according to ARPA Piemonte studies, its return period was greater than 200 years. The other remarkable events occurred in November 1962, October 1979, October and November 2000 and November 2002. However, their temporal rainfall distributions differ (Fig. 5a) from those that occurred in November 2016. It is important to note that the cumulative rainfall that occurred in the 30 days before the 2016 event was not as significant as that associated with the rainfall events of October and November 2000, which triggered landslides nearby Monesi di Triora (Federici et al. 2007) (Fig. 5b). The 1994 event, known as one of the most severe events in southern Piedmont, resulted in this area being less significant than the other events. Regarding the snow records, only the dataset from 1999 is available. However, as most of the extreme rainfall occurred in autumn, the role of snow melting can be considered negligible.

November 2016 event

Ground effects at the basin scale

From 20 to 25 November 2016, heavy rainfall affected the northwestern part of Italy. For several days, a deep low-pressure cyclone was blocked in the western Mediterranean Sea, creating favourable conditions for heavy rain in the Liguria region. The storm activated steady wet streams from the SE that to the Alps, causing heavy and persistent rainfall (ARPA Piemonte and Regione Piemonte 2018). This event caused one of the more major floods in the Piemonte and Liguria regions that have occurred in recent decades, resulting in inundation along the Tanaro and Po rivers (Notti et al. 2018; Giordan et al. 2018). This sector of the Ligurian Alps was particularly affected by heavy rainfall, and many rain gauges measured cumulative values much higher than those registered during the past major extreme rainfall events of November 1994 and October 2000 (ARPA Piemonte and Regione Piemonte 2018). This critical precipitation lasted from the afternoon of 20 November until 25 November. The rainfall was mainly concentrated from 23 to 25 November. A peak of 30 mm/h was registered in the late morning of 24 November. The accumulated rainfall reached 691 mm, which was confirmed by nearby stations (Fig. 6b). This meteorological station (managed by ARPA Piemonte) was located approximately 2 km WSW from Monesi di Mendatica on the south flank of the Bavera valley at 1600 m a.s.l.

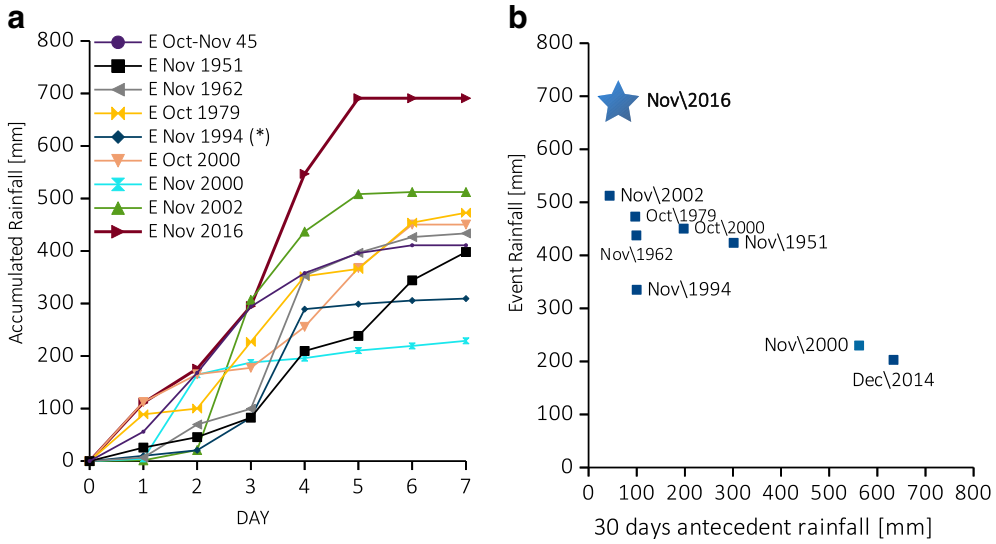

Fig. 5 The extreme rainfall event of 2016 compared with the main events (E) that have occurred since 1951. **a** The accumulated rainfall and **b** scatterplot of rainfall events and 30-day antecedent rainfall. (*) In 1994, the closest pluviometer was located at the Upega gauge, located 9 km N of Monesi.

According to our analysis of various high-resolution satellite datasets (Pleiades, Google Earth and Sentinel-2), this rainfall event triggered many shallow landslides (approximately 40 over 11 km² in the study area, Fig. 6a). Many shallow and deep-seated landslides also occurred in the rest of the upper Tanarello basin and in the upper Arroscia Valley (Pepe et al. 2019). Some of them were related to the collapse of old terraces, as had already occurred in other places of the Liguria region after extreme rainfall events (Guzzetti et al. 2004; Giordan et al. 2017a). The debris mobilized from the shallow landslides and eroded stream banks contributed to debris flows and hyperconcentrated floods that ran for some kilometres in the Bavera-Tanarello stream beds (DF1 Fig. 4a) until it was blocked by the deposits of the Monesi rotational landslide (L1 in Fig. 6a). As a consequence, approximately 10 m of debris was deposited in the riverbed of the Tanarello stream upstream of Monesi.

During the same event, a few deep-seated landslides were activated in the upper Tanarello basin: (1) a complex landslide near Monesi di Triora (L4 in Fig. 4a), (2) an incipient rotational landslide in the village of Piaggia (L3 in Fig. 6a), and (3) a rotational landslide and (4) a deep-seated planar landslide, both (3-4) in the village of Monesi di Mendatica (L1 and L2 in Fig. 4a). Additionally, the village of Piaggia was also hit by rapid earthflow (ARPA Piemonte and Regione Piemonte 2018).

Landslides L1 and L2 were the most destructive, and they severely affected the village of Monesi di Mendatica. The rotational landslide L1 had a volume of 7–9 10^4 m³ and was probably triggered by the erosion of the Tanarello stream at the toe of the slope. This landslide destroyed a section of the provincial road and caused the collapse of two buildings in the village. The landslide deposits partially dammed the Tanarello stream and stopped the previously mentioned debris flow (DF1).

The second landslide that occurred in Monesi was a deep-seated planar landslide L2. Its area was approximately 0.4 km² and its estimated volume was 8–1210 ^{6} m³. After the November 2016 extreme rainfall event, this landslide experienced an estimated movement up to 4 m in a few days. The reactivation of this ancient landslide damaged most of the buildings and structures in the village, and several cracks and trenches appeared at the boundary of active areas.

Monesi di Mendatica is mainly a touristic resort for the nearby ski station. During the 20–25 November 2016 event, only a few people occupied the buildings, and fortunately, they all left before the catastrophic phase of the landslide, thus avoiding fatalities.

Chronological evolution of catastrophic phase

Based on the gathered data, we could indicate that the catastrophic phase of the landslide event lasted 4–5 days. In the following, we present the reconstructed event chronologically, as reported in Fig. 7 and mapped in Fig. 8:

1. Event 1 (E1 in Fig. 7). The event started with the partial activation of rotational landslide L1 (Fig. 6 and photo 1a in Fig. 8), which occurred in the early morning of 24 November 2016 when the rainfall intensity reached a peak of 35 mm/h, and the cumulative rainfall reached 500 mm. In this phase, the erosion of the Tanarello stream at the toe of the slope probably contributed to triggering the rotational landslide (L1). The landslide affected an old mill, a building of a small hydroelectric plant and an electric trellis. The landslide deposit partially dammed the Tanarello stream. Several springs related to a massive increase in the piezometric level in the landslide body appeared in the lower sector of the landslide (photo 1 b in Fig. 8). The small Bandita Creek flooded the slope near Monesi and could have contributed to the water pressure increase in the landslide body. At the same time, several shallow landslides contributed to debris flows along the Bavera-Tanarello streams (photo 1c in Fig. 8). This debris flow (estimated volume ≈ 5–10 10^4 m³) was blocked by the deposit of rotational landslide L1. The Tanaro River at the Ponte di Nava

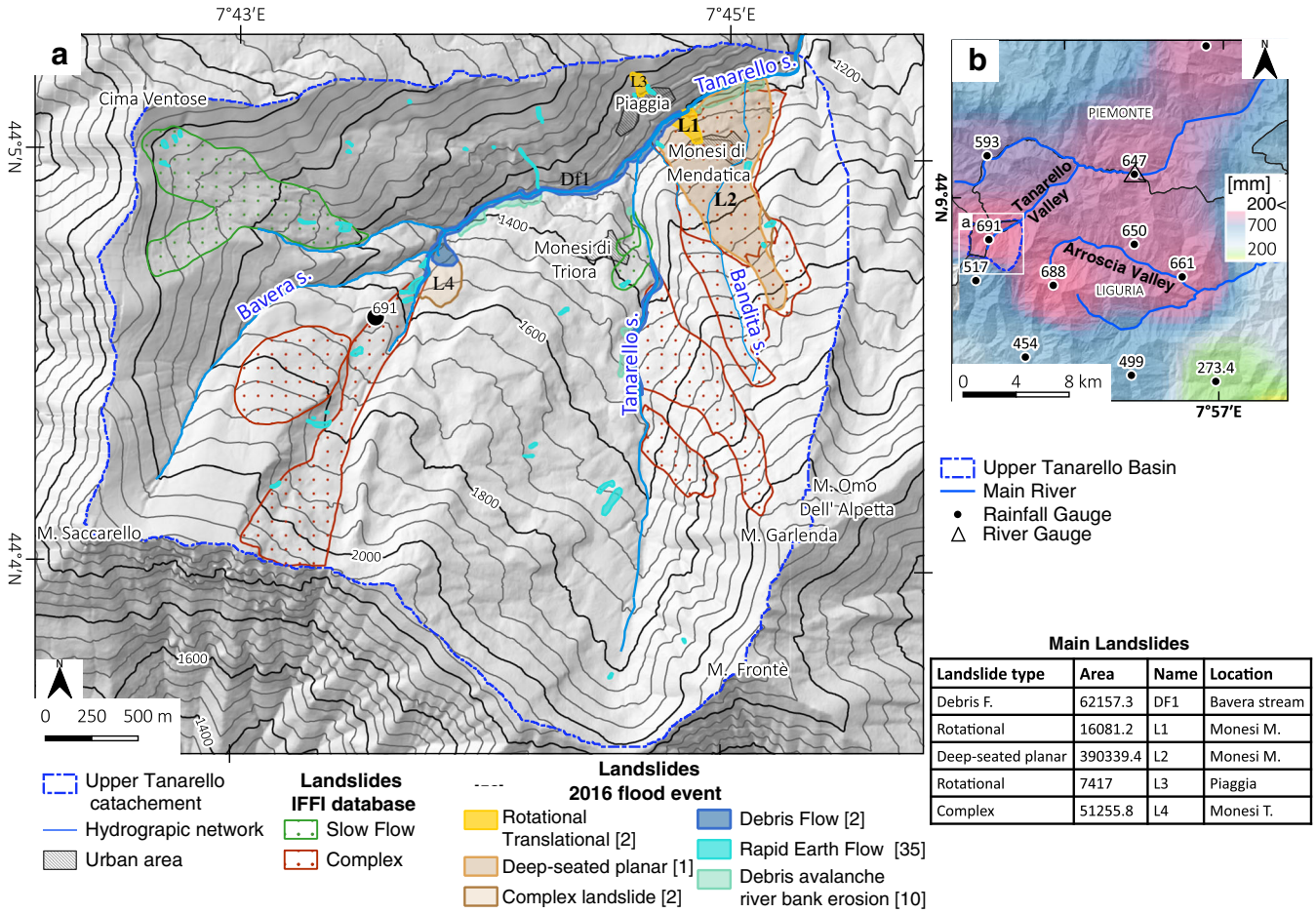

Main Landslides

Landslide type	Area	Name	Location
Debris F.	62157.3	DF1	Bavera stream
Rotational	16081.2	L1	Monesi M.
Deep-seated planar	390339.4	L2	Monesi M.
Rotational	7417	L3	Piaggia
Complex	51255.8	L4	Monesi T.

Fig. 6 **a** Event map of the 2016 flood event for the upper Tanarello catchment. **b** Five-day cumulative rainfall measured at the closest meteorological stations

gauge (approximately 12 km downstream of Monesi) reached a level of 400 cm and a maximum discharge of 450 m^3/s. We estimated that at the base of the catchment area for the Tanarello stream in Monesi, the discharge peak was approximately 30–40 m^3/s. The flood peak passed 1 h in advance with respect to the Ponte di Nava gauge.

2. Event 2 (E2 in Fig. 7). During the night between 24 and 25 November, the second highest peak (≈ 25 mm/h) of rainfall intensity was registered. The accumulated rainfall reached up to 700 mm. Additionally, the second highest discharge peak of the Tanrello stream occurred. The first signs of deep-seated planar landslide reactivation (L2) appeared on both flanks of the landslide with scarp exposure up to 70 cm (photos 2a and 2b in Fig. 8). At this point, the building started to crack, and the pylons of the electric line tilted. The rotational landslide (L1) maintained its retrogressive movement.
3. Event 3 (E3 in Fig. 7). During the night between 25 and 26 November, one day after the rainfall event, the further failure of landslide L1 continued with a retrogressive trend. This failure (with a cumulative displacement of 40 m) destroyed the main road of the village and severely damaged two buildings, which finally collapsed a few weeks later (photo 3a in Fig. 8). The cracks on the rest of the buildings considerably increased.
4. Event 4 (E4 in Fig. 7). According to the presented event reconstruction, most of the displacement of L2 occurred from 24 to 27–29 November, with an estimated displacement up to 4 m. Field surveys, performed on 6 December 2016 (photo 4a in Fig. 8) by the ARPA Piemonte (ARPA Piemonte and Regione Piemonte 2018), did not confirm any significant movement, so the catastrophic phase was considered terminated. The surveys also show that the landslide boundary was delimited by sharp cracks and that the landslide movement at the crown was up to 10 m.

Coevent displacement with DIC and manual measure

We used DIC and manual analysis to obtain the coevent displacement of the L2 landslide. In Fig. 9, we present the computed planar displacement for the following input images obtained from (i) the Planet satellite (Fig. 9a) and (ii) Sentinel-2 satellites (Fig. 9b).

DIC outputs showed that the mean horizontal displacement was approximately 2.5 ± 1 m NNW (≈ 340°N) for both the Sentinel-2 and Planet satellites (Fig. 9 a and b). Figure 9 d shows a Q-Q plot that compares the displacement measured with Planet and Sentinel-2. In this picture, the displacement derived from the

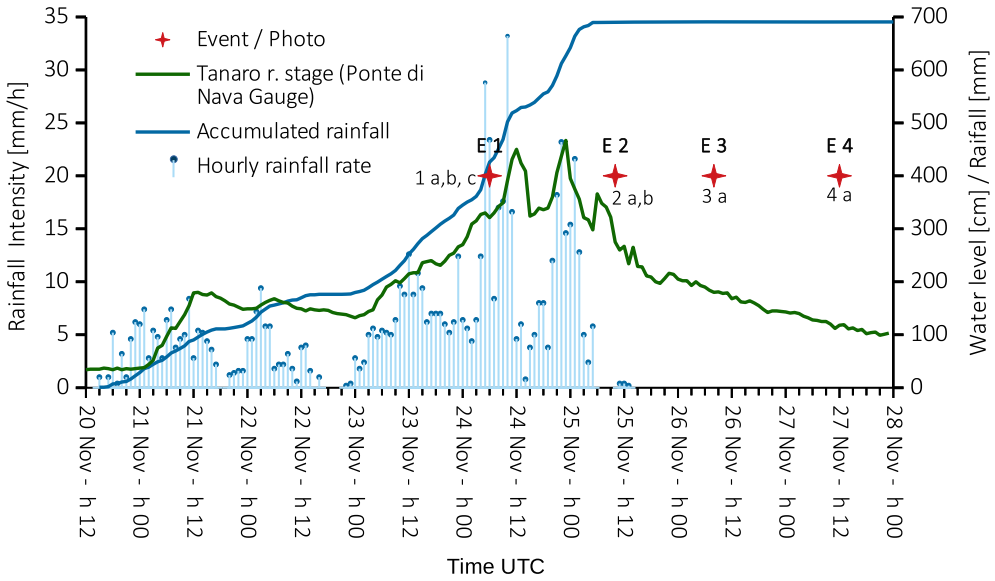

Fig. 7 Hourly and accumulated rainfall at the Piaggia Station compared with the Tanaro stream level at the Ponte di Nava gauge. The main events (E1–E4) and the corresponding chronologically documented photographs (1–4) are reported in Fig. 8

Planet imagery was slightly larger, especially that of the lower values. This was probably due to the finer spatial resolution of the Planet images (Fig. 9d). The finer resolution of Planet images also allowed us to better identify the shape of the area with the highest displacement (up to 4 ± 1 m) that was located in the central and upper parts of L2.

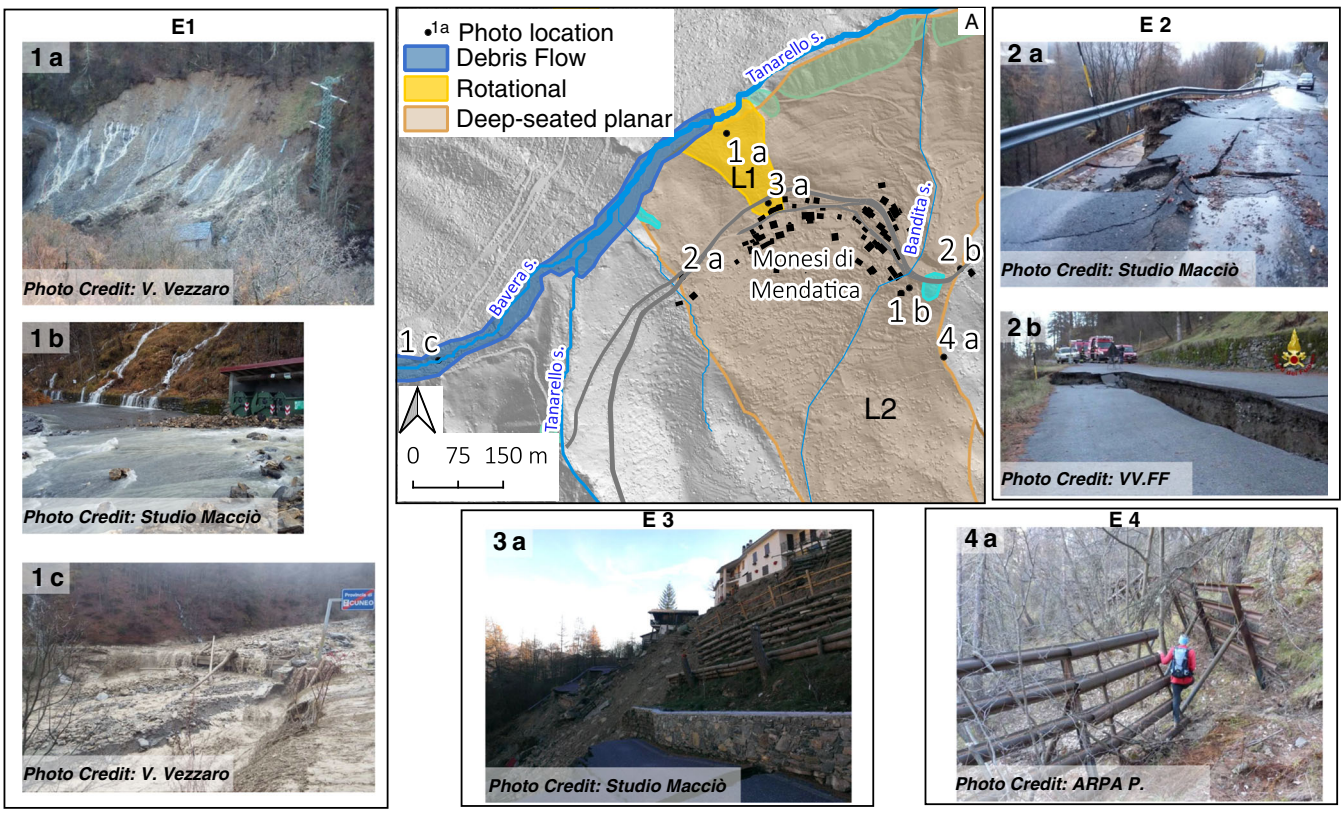

Fig. 8 Representative photographs of the principal events (**E 1**–**E 4**) chronologically documented (1–4) marked on map A and in Fig. 7. **1 a** Initiation of the collapse of L1. **1 b** Rise of groundwater table and widespread springs flood and shallow landslides. **1 c** Debris flow (DF1). First fractures on the southwest (**2 a**) and northeast sides (**2 a**) of L2. **3 a** Total collapse of the rotational landslide and **4 a** end of main displacement of the large deep-seated planar landslide

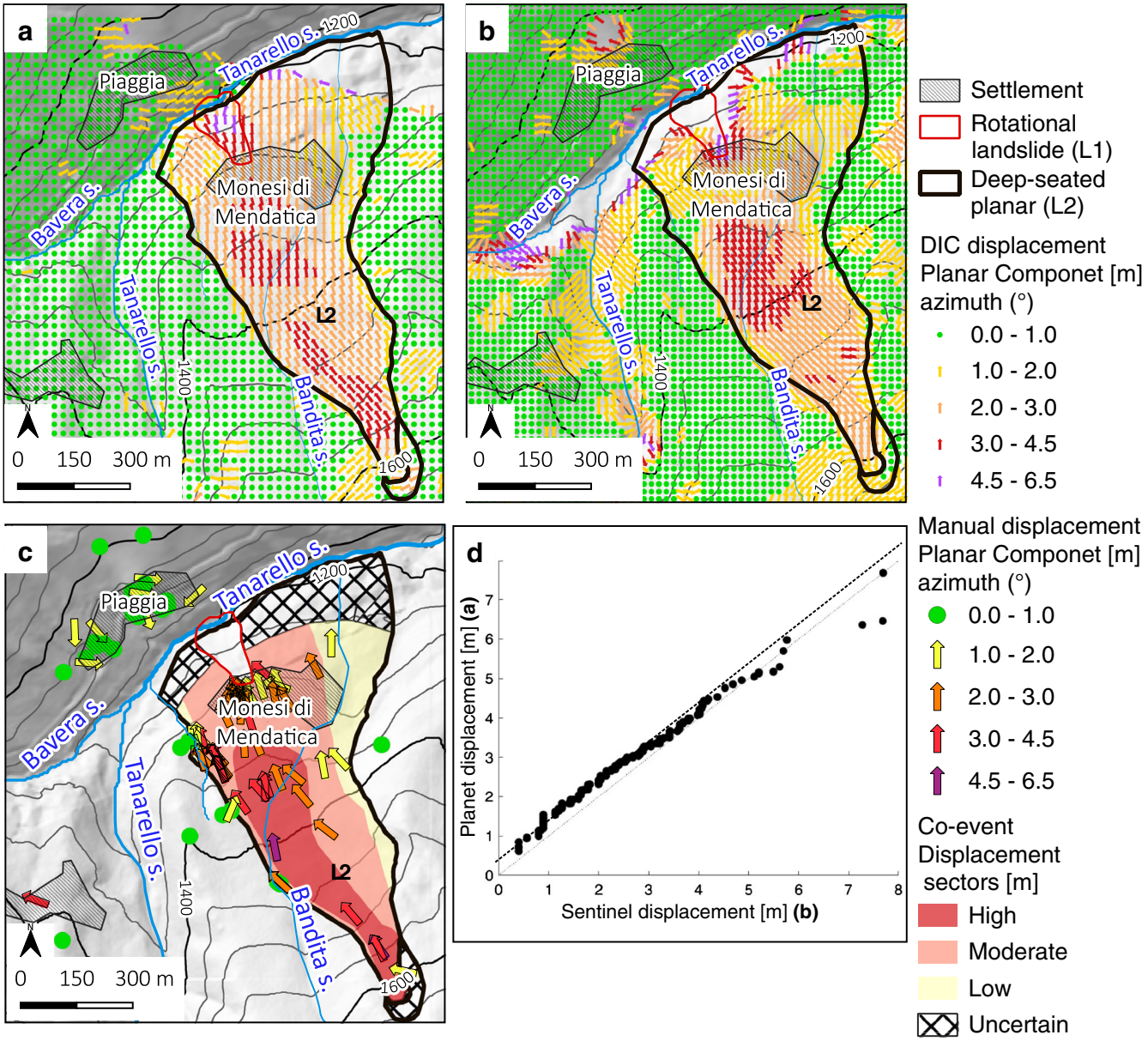

Fig. 9 Planar displacement resulting from digital image correlation (DIC) based on **a** Planet satellite images and **b** Sentinel-2 satellite images. **c** Deep-seated planar landslide L2 divided into three sectors of coevent displacement intensity based on the DIC results and manual measurement of movement and azimuth. **d** Q-Q plot of the 2-D displacement obtained with DIC using Sentinel and Planet data. The dashed line indicates the 1:1 correspondence

We compared the manually computed displacement with the displacement obtained by the DIC technique (Fig. 9c), and the results were in good agreement. We noted that manual measurements might be affected, as in the case of the DIC technique, by noise related to shadow length, image distortion and orthorectification errors (the expected noise was approximately ± 1 m).

Based on the obtained coevent displacement, we could define three landslide sectors as presented in Fig. 9c: low (< 2), moderate (2–3 m) and high (> 3 m). These sector boundaries were established using the DIC results and the manual measurement of displacement. Regarding the toe and crown of the landslide, it was not possible to define displacement classes for these parts of the landslide.

The DIC results show sporadic false-positive displacement in stable areas. Several causes could explain the noise of the measurement obtained in stable regions: (i) variation of the terrain reflectance related to changes in vegetation activity and anthropic work or shallow landslides; (ii) differences in the shadow length and directions caused by the sun's position; (iii) image deformation related to orthorectification processes. In the case of Sentinel-2, the detected movement was close to the DIC sensitivity because the displacement was much lower the

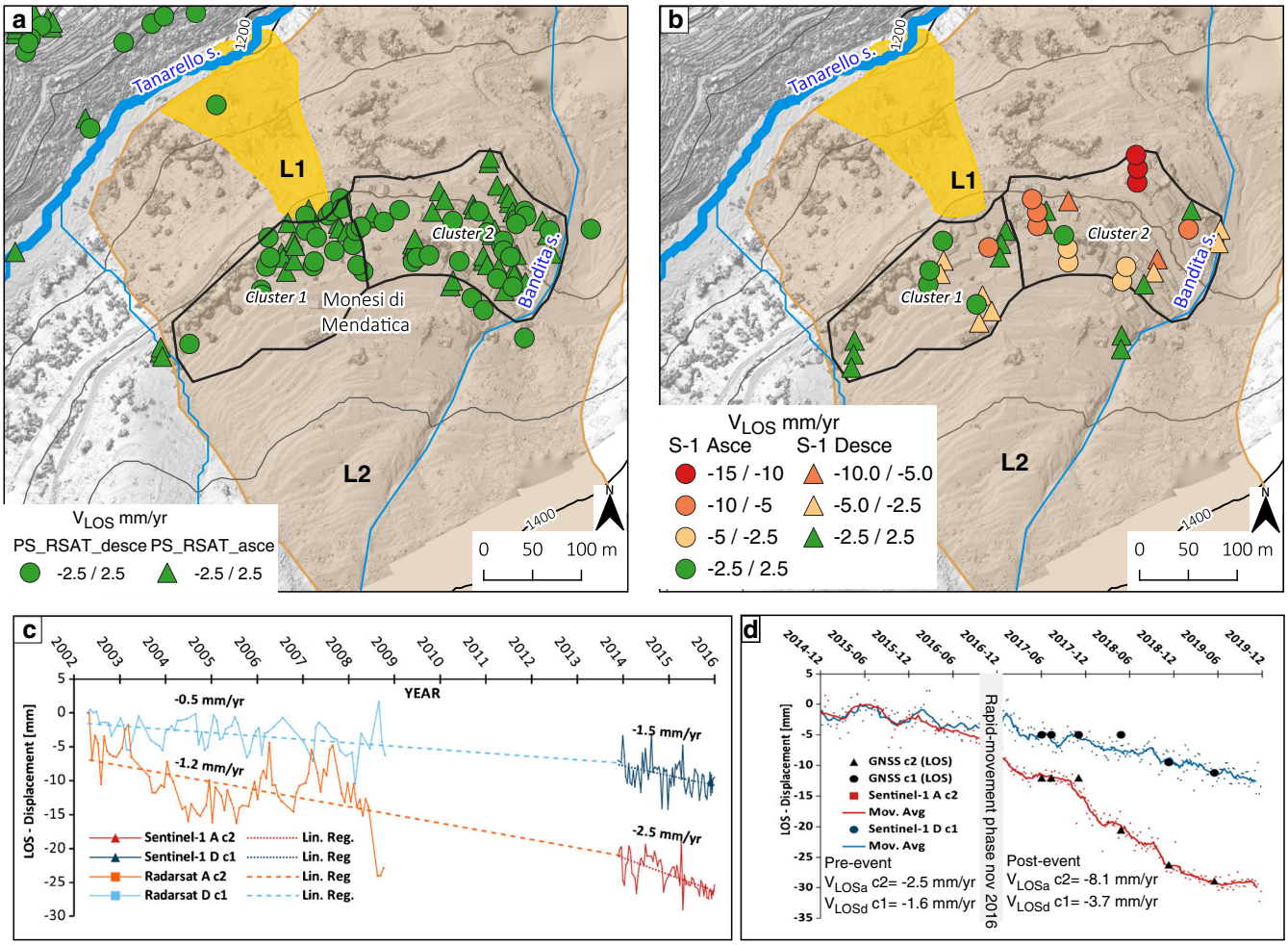

Fig. 10 Maps of the PSInSAR velocity. We grouped the data into two clusters based on the slope aspect to analyse the time series. **a** The VLOS for the ascending and descending Radarsat satellite datasets. **b** The VLOS for the ascending and descending datasets of the Sentinel-1 satellites. **c** Time series of Radarsat and Sentinel-1 until November 2016 event. **d** Time series of Sentinel-1 and GNSS (black marks) are compared for both clusters. Pre- and postevent velocities are also calculated

spatial resolution of the satellite images (approximately one fourth). In the bottom sector of the landslide, near the Tanarello stream, the DIC failed because the rotational landslide collapse (L1) and other shallow landslides caused image decorrelation effects.

Reconstruction of the 2003–2019 landslide velocity with InSAR data

We obtained pre- and postevent displacements by interpreting InSAR datasets already processed with the SqueeeSAR algorithm (Ferretti et al. 2011). Using the Sentinel-1 data, we were able to estimate the landslide activity until a few days before the November 2016 event and its postevent displacement until December 2019. Regarding the catastrophic phase, the landslide evolution (displacement up to 3 m) was too rapid for detection by the InSAR technique. We must also consider that the slope orientation of this study area faced towards the north, which was not favourable for InSAR analysis. The satellite along the line of sight (LOS) could detect less than 50% (i.e. C = 0.5, Notti et al. 2014; Béjar-Pizarro et al. 2017) of the real displacement for this slope orientation.

In Fig. 10, we present the LOS velocity map (Fig. 10 a and b) and the displacement time series of Radarsat (2003–2009) and Sentinel-1 (2014–2019) (Fig. 10 c and d). We grouped the results into two clusters based on their slope aspect: cluster 1 faced NNW, which was better represented by the descending dataset, and cluster 2 faced NNE, which was better represented by the ascending dataset.

The pre-event InSAR data of both Radarsat and Sentinel-1 allowed us to analyse the period from 2003 to November 2016. The cumulative displacement derived from the InSAR time series analysis along the line of sight (LOS) was less than 30 mm for cluster 2 and less than 15 mm for cluster 1 (Fig. 10 c). The V_{LOS} values for Radarsat were smaller than those for Sentinel-1. Moreover, the V_{LOS} for both satellites projected along the slope (V_{SLOPE}) indicated some slight movements in the NE sector of the village (< 5 mm/year). These data agreed with the ground and geomorphological observations.

The analysis of these time series shows unexpected results, i.e. the average trend seemed to slightly accelerate after the 2016

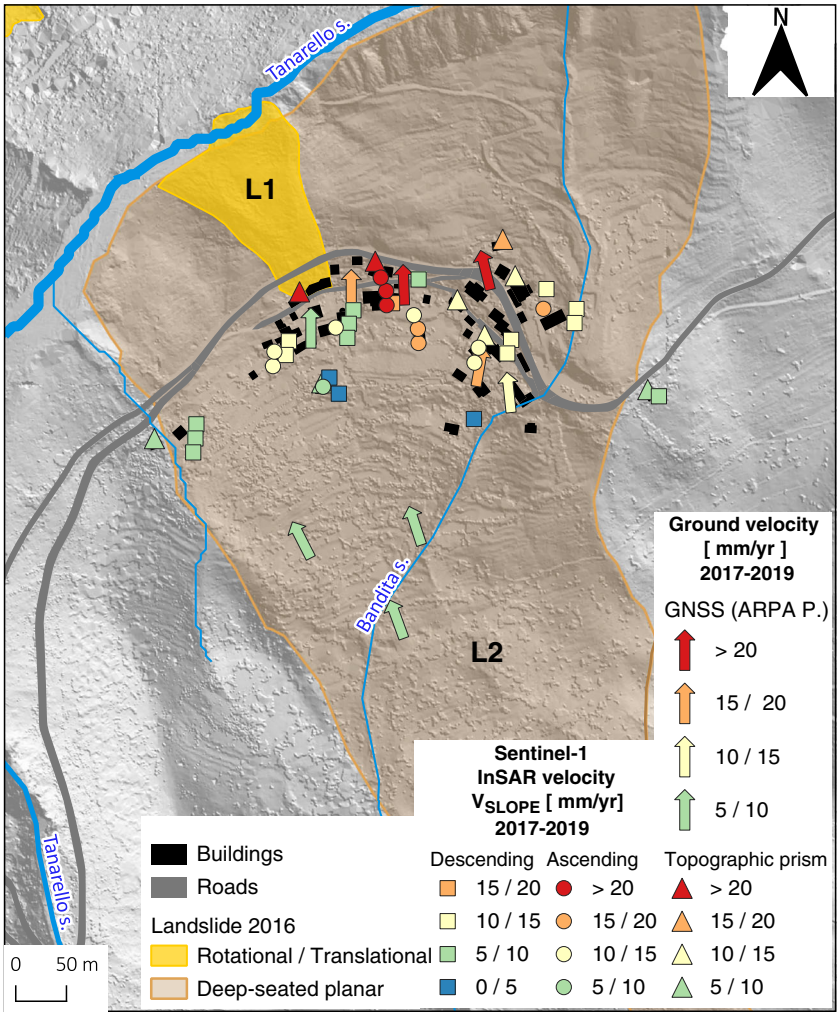

Fig. 11 Postevent velocity of the Monesi Landslide from in situ instruments and InSAR data (projected along the slope)

event. Even if the time series after the event of 2016 were limited, the use of GNSS campaigns conducted from 2017 to 2019 supported the presented results. The GNSS measurements were projected and rescaled along the LOS to compare them with the SAR data. More details about the GNSS network are presented in the postevent monitoring results section. According to Fig. 10d, we observed some variability in the postevent displacement rate. This may have been related to rainfall and groundwater level oscillations. However, more extended time series and analysis would be necessary to establish if this trend was related to a real change in kinematics or to a velocity oscillation shift related to seasonal trends or alternations of dry and rainy periods already existing before the 2016 catastrophic phase. Moreover, the area with the highest postevent velocity detected by SAR (≈ 10 mm/year LOS) was located in the NE sector (cluster 2), as already shown by the Radarsat data (Fig. 10a). During the catastrophic phase of November 2016, the highest displacement values were located in the central and western sectors of the landslide (Fig. 9).

Postevent monitoring results

Topographic postevent displacement monitoring results

In Fig. 11, we plotted the results of 2 years of postevent displacement monitoring. We elaborated the measurement data from the nine GNSS benchmarks (of ARPA Piemonte) and nine topographic prisms. In this figure, we also present the postevent InSAR data projected along the slope. The results showed an agreement between the two monitoring systems (GNSS and topographic) and the InSAR data; the highest velocities (up to 25 mm/year) were located in the lower NE sector of the landslide, while the lowest values were located in the central and western sectors. The spatial velocity distribution coincided with the pre-event data (Fig. 3).

The inclinometric measurements did not seem reliable. This may be related to incorrectly installed inclinometric tubes resulting from the landslide mass composition, i.e. the presence of large blocks. Only the S1 inclinometer, located in the eastern sector of the landslide, seemed to provide a reliable velocity of 19 mm/year at a depth of approximately 42 m at the contact between

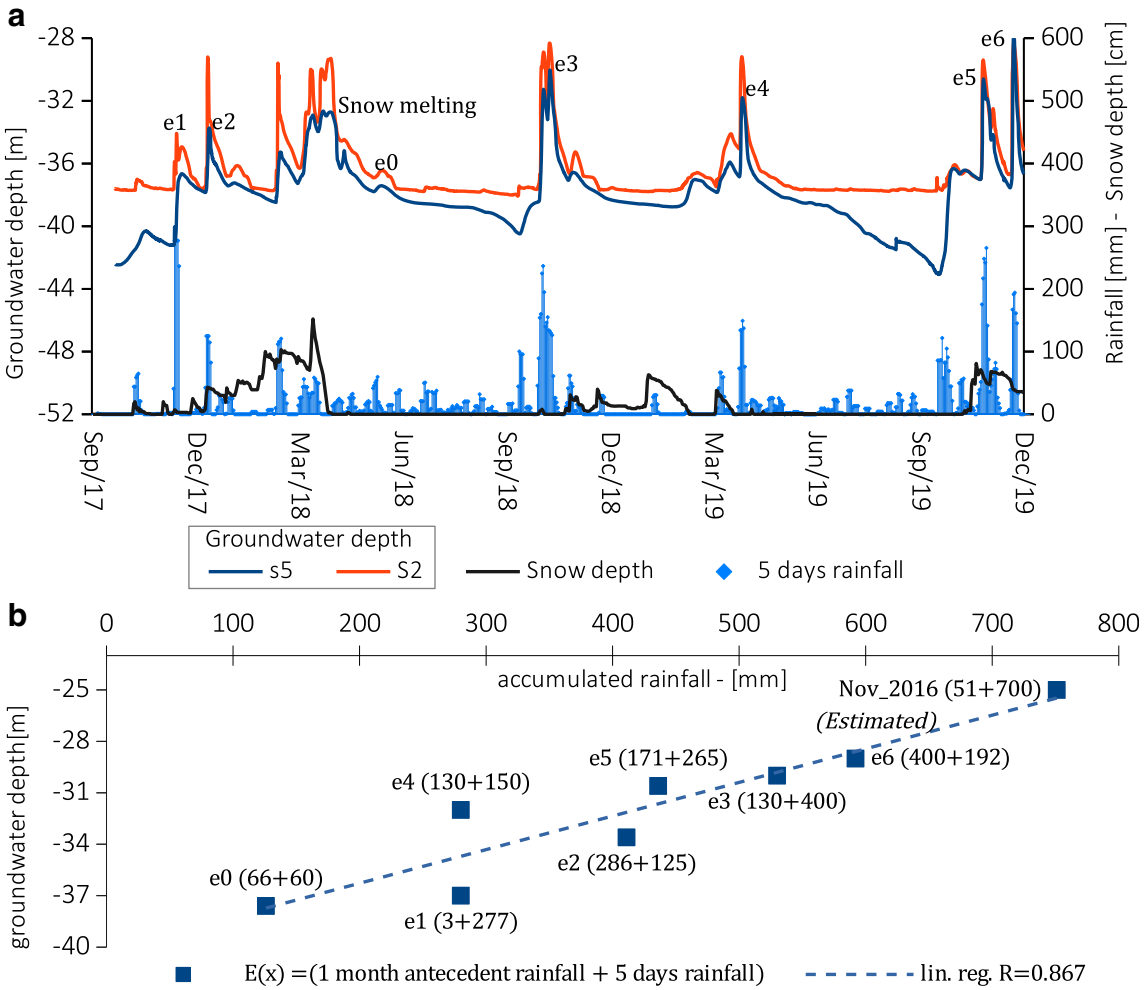

Fig. 12 Postevent piezometric data. **a** 5-day accumulated rainfall, snow depth and water depth for piezometers S5 and s2. **b** Linear regression of groundwater level based on seven rainfall events that occurred from November 2017 to November 2019. Event e0 is an example of weak-moderate rainfall (60 mm) that caused a negligible increase in the groundwater level (0.3 m)

the landslide body and the bedrock. This measure was comparable with surface monitoring. In addition to in situ instruments, we also used the Sentinel-1 SqueeSAR™ data already discussed in the InSAR results paragraph. In Fig. 11, we plotted the postevent velocity projected along the slope (V_{SLOPE}) of both ascending and descending Sentinel-1 datasets.

The rotational landslide (L1) was not subject to any continuous monitoring, but some short experimental GB-SAR monitoring campaigns were performed in 2017 and 2018 (Luzi and Dematteis 2019). We could only estimate the displacement by comparing the pre- and postevent DTMs and analysing the aerial photographs. We obtained a vertical movement estimate up to 15 m and a horizontal movement up to 30 m (see supplementary materials).

Piezometric data and correlation with rainfall and snow melting

The piezometric data cover the period from November 2017 to November 2019 for piezometers S2 and S5 (see Fig. 12). We compared the piezometric level with the 5-day cumulative rainfall and snow depth (at 1600 m a.s.l.) (Fig. 12a). We identified five main events (e1–e5 in Fig. 12) of notable groundwater level increase that were related to the heavy rainfall events that occurred from November 2017 to November 2019. We noted the effect of the already saturated terrain related to snow melting (e2 in January 2018) or close antecedent rainfalls (e6 in December 2019). In both cases, the increase in groundwater level was faster and more robust than for the events that started in dry conditions. Concerning the snowmelt, its effect was evidenced by the piezometric increase observed in spring 2018, when approximately 1.5 m of snow rapidly melted, and in consequence, the groundwater level increased by approximately 4 m without any contribution from the intense rainfall events.

We used postevent piezometric data (not related to snowmelt) to estimate the water table level in November 2016 using linear regression, as the results (e1–e6) showed a linear distribution (Fig. 12b). We applied linear regression to the sum of rainfall events (5 days) with the 30-day antecedent rainfall compared with the maximum level reached by the groundwater. According to this analysis, the piezometric level for the event of November 2016 reached an estimated value of 24–26 m below ground level.

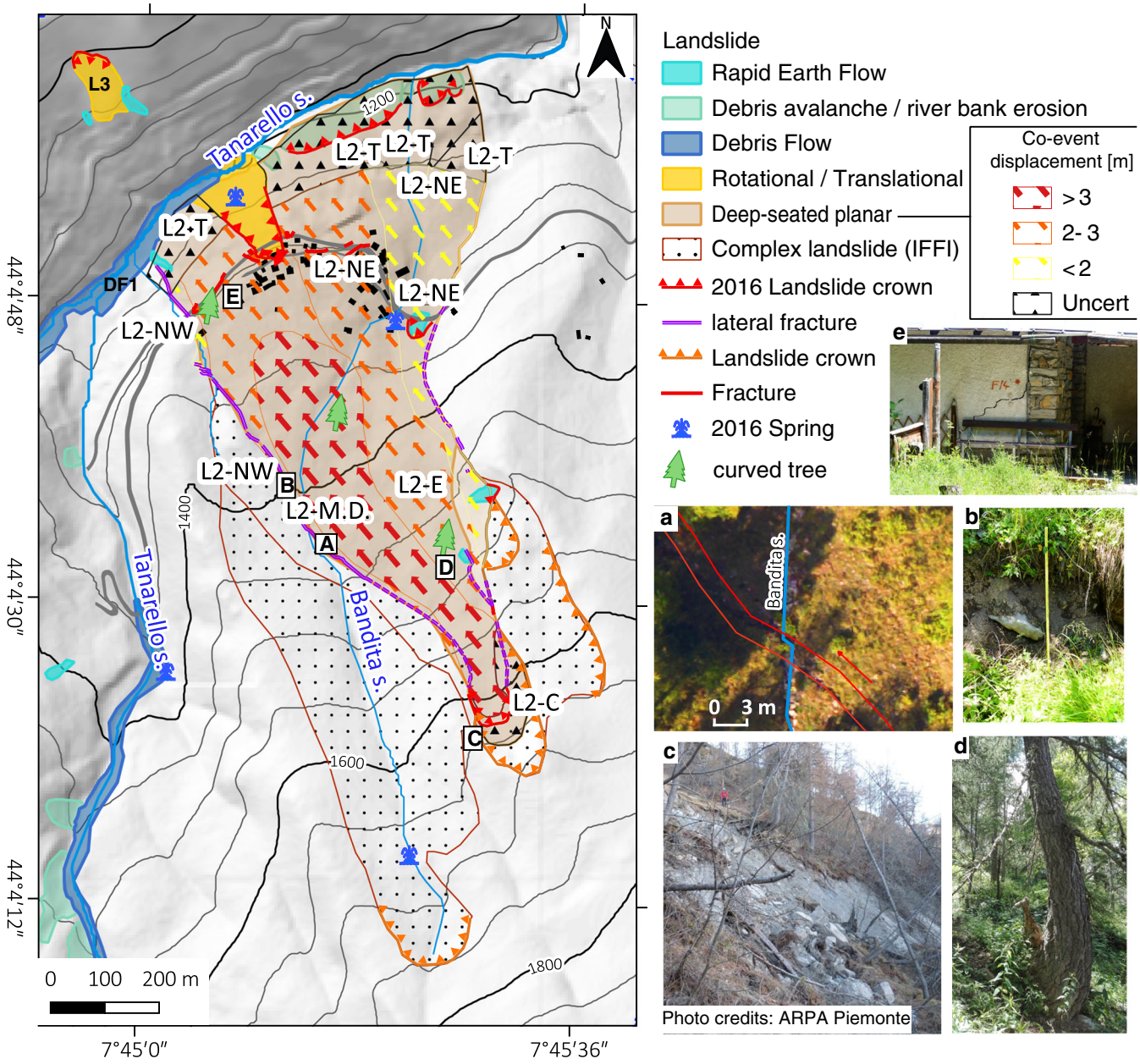

Fig. 13 Geomorphological map of the Monesi landslides. **a** Details of the deviation of the Bandita stream on the left flank of the landslide. **b** Detailed view of a fracture on the left flank, with a vertical slip of 0.7 m. **c** Crown of the reactivated landslide, with displacement up to 10 m. **d** Curved tree in the central sector of the landslide. **e** Centimetric crack on a building in the L2-NW sector

We observed that during the main events, the maximum groundwater level occurred 24–36 h (piezometer S2) and 48–60 h (piezometer S5) after rainfall events.

Geomorphological mapping and damage assessment

Based on the results obtained with the DIC technique (§ coevent displacement with DIC and manual measure), postevent monitoring data (§ Topographic postevent displacement monitoring results) and field surveys, we defined six sectors of the L2 landslide using an approach based on the definition of morpho-structural domains (Giordan et al. 2017b) (Fig. 13):

- The toe of the landslide (L2-T) was characterized by a steep slope (> 30°). L2-T was also affected by the rotational landslide (L1) and other shallow landslides. For this sector, the DIC technique could not detect any displacement due to interference from noise.
- In the NE sector (L2-NE), DIC detected a moderate displacement of 2 m and postevent monitoring registered a slow velocity (≈ 20 mm/year). In this sector, moderate to severe building damage was observed.
- In the NW sector (L2-NW), DIC detected a moderate displacement of 2 m and postevent monitoring registered an extremely

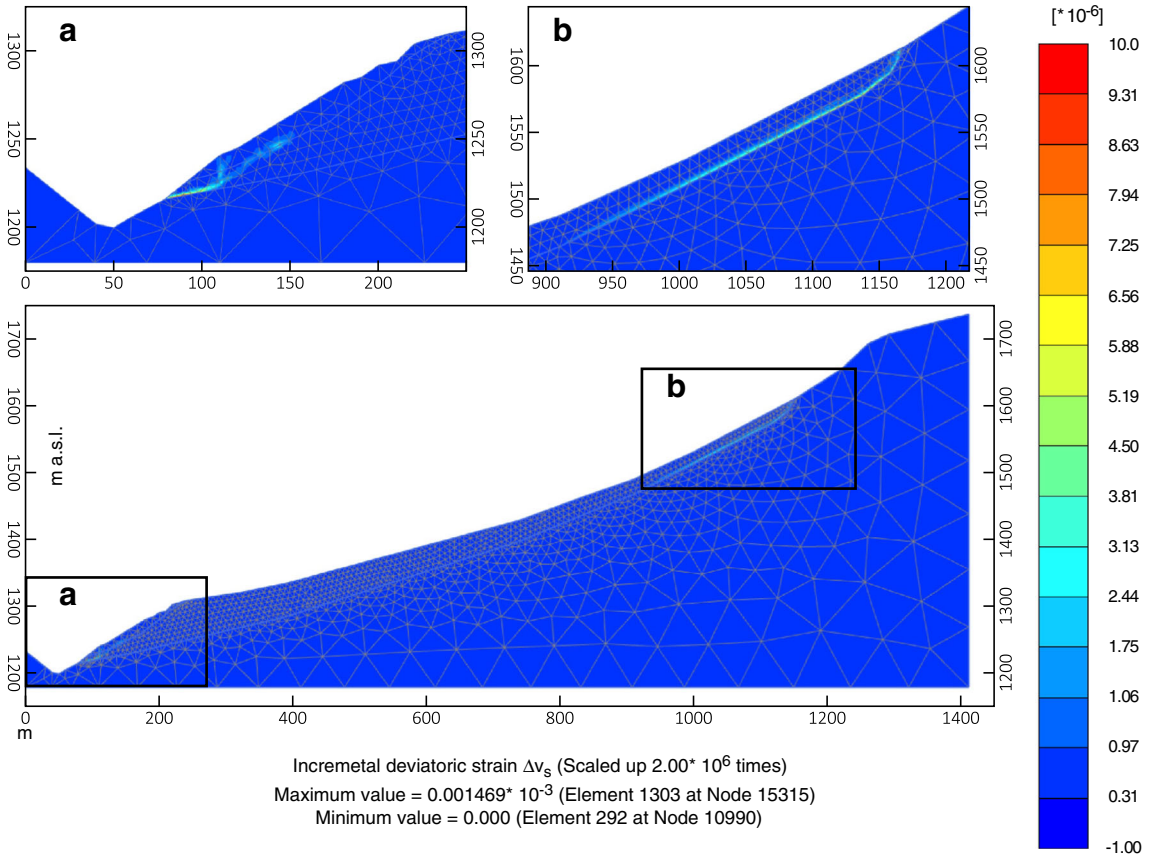

Fig. 14 Pre-event model; contours of the incremental deviatoric strain obtained for the critical GWL (25 m below ground level). **a** Detail of the incremental deviatoric strain at the bottom of the slope (rotational landslide L1). **b** Detail of the incremental deviatoric strain at the crown of landslide L2

slow velocity (< 10 mm/year). In this sector, severe damage to the building was observed.

- In the eastern sector (L2-E), DIC detected a displacement of 1–2 m and where geomorphological signs of movement are weak.
- In the central sector of the deep-seated planar landslide (L2-H.D.), DIC detected a significant displacement of 3–4 m. For this sector, post-monitoring data were not available, but the geomorphological traces of movement were notable.
- In the sector where the crown of the reactivated landslide (L2-C) had an estimated movement up to 10 m, DIC was not able to detect any movement due to the dense vegetation, strong vertical component and limited area (Fig. 13c).

The most definite signs of L2 activity were fractures that appeared along most landslide perimeters and were also visible in the high-resolution aerial images. The fractures showed vertical displacements of approximately 0.5–1 m affecting colluvial and landslide deposit material (B). Lateral fractures were more evident on the southwest flank of landslides where the displacement reached higher values with respect to the right side.

At the landslide crown, a movement up to 10 m was measured by the ARPA Piemonte during field surveying in December 2016 (Fig. 13c). At the crown, the bedrock outcrops and the bedding of the San Remo Flysch Formation were favourable to slope instability. From high-resolution aerial photography (Fig. 13a), we detected the deviation of the Bandita stream on the left lateral landslide boundary. It is interesting to note that this stream, before crossing L2, was parallel to the landslide boundary for approximately 100 m (Fig. 13).

The field survey shows horizontal displacement up to 2 m along the lateral boundaries, in agreement with the DIC and aerial photo results. Some shallow landslides were also visible on the right lateral side of the main landslide. The left flank of landslides presented a sharper boundary with evident fractures, while the boundary on the right flank was less defined. A field survey allowed us to map the damages to buildings and infrastructure that occurred in Monesi. We used the scale proposed by Cooper (Cooper 2008), which enabled a rapid and qualitative evaluation of damage based on a rapid field survey. In general, we observed that most of the buildings located within the L2 landslide were damaged. The degree of damage increases in the central part of the landslide but with a random distribution, likely related to building structure and foundation factors. Two buildings located on rotational landslide L1 and the hydroelectric power plant collapsed. Roads and retaining walls showed widespread damage with fractures and displacement up to 0.5–1 m.

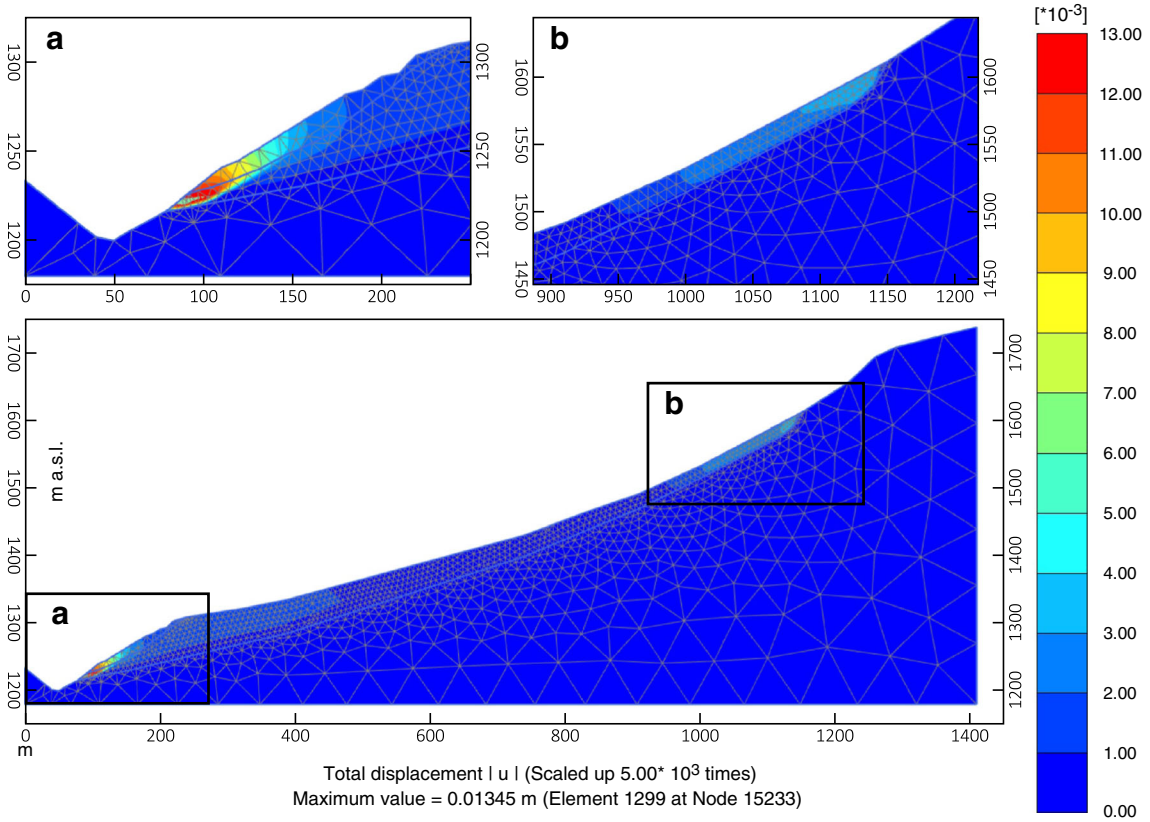

Fig. 15 Pre-event model; contours of the accumulated displacement obtained for the critical GWL (25 m below ground level). **a** Detail of the accumulated displacement at the bottom of the slope (rotational landslide L1). **b** Detail of the accumulated displacement at the main scarp of L2

Results of numerical modelling

Based on the numerical results, we derived an interpretation of the slope stress-strain behaviour and inferred the variation in the safety factor as a function of the GWL. In particular, assuming a groundwater level of approximately 25 m below ground level (the maximum groundwater level inferred as a consequence of the rainfall event), we did not obtain a numerical convergence in the plastic calculation, but we were able to calculate the corresponding safety factor, which was equal to 1.01. (Fig. 14). A clear failure mechanism at the toe of the landslide was observed in this analysis (Fig. 14a), with a displacement field that was initiated in the lowest part of the landslide at the contact between the landslide debris and the bedrock (Fig. 15a) and then propagated upwards within the debris mass (Fig. 14b and Fig. 15b). These numerical results agreed with the field observations, as well as the satellite data and DIC analyses, which highlight that the highest displacement values were concentrated in the lowest portion of the slope, where the rotational landslide (L1) occurred (Fig. 15a). Regarding the influence of GWL, we obtained a progressive increase in the safety factor with the lowering of the GWL (Table 6), which indicated that an exceptionally high groundwater level (i.e. 25 m below ground level) was capable of triggering the observed failure process. We also noted that the numerical results, in terms of displacements of the pre-event case, closely follow the new post-landslide profile defined on site (Fig. 3b).

Table 6 Estimated safety factor (SF) for various piezometric levels in accordance with the strength reduction method

Groundwater level from the surface (m)	Estimated SF
− 43	1.58
− 40	1.55
− 37	1.48
− 34	1.43
− 31	1.27
− 28	1.17
− 25	1.01

The analysis concerning the impact of L1 failure on the general stability of the slope suggests that for such a configuration of the model, numerical convergence is reached, which means that no failure condition is obtained. However, a straining process remains active in the lowest part of the slope (Fig. 16a, b), along with moderate incremental deformation that appears near the crown of the L2 landslide (Fig. 17a, b).

Discussion

Extreme rainfall is among the main landslide triggering factors. For instance, Gallus Jr et al. (2018) forecasts that in the coming years, the frequency of these events will increase due to global warming, especially in the autumn season near the Ligurian Sea.

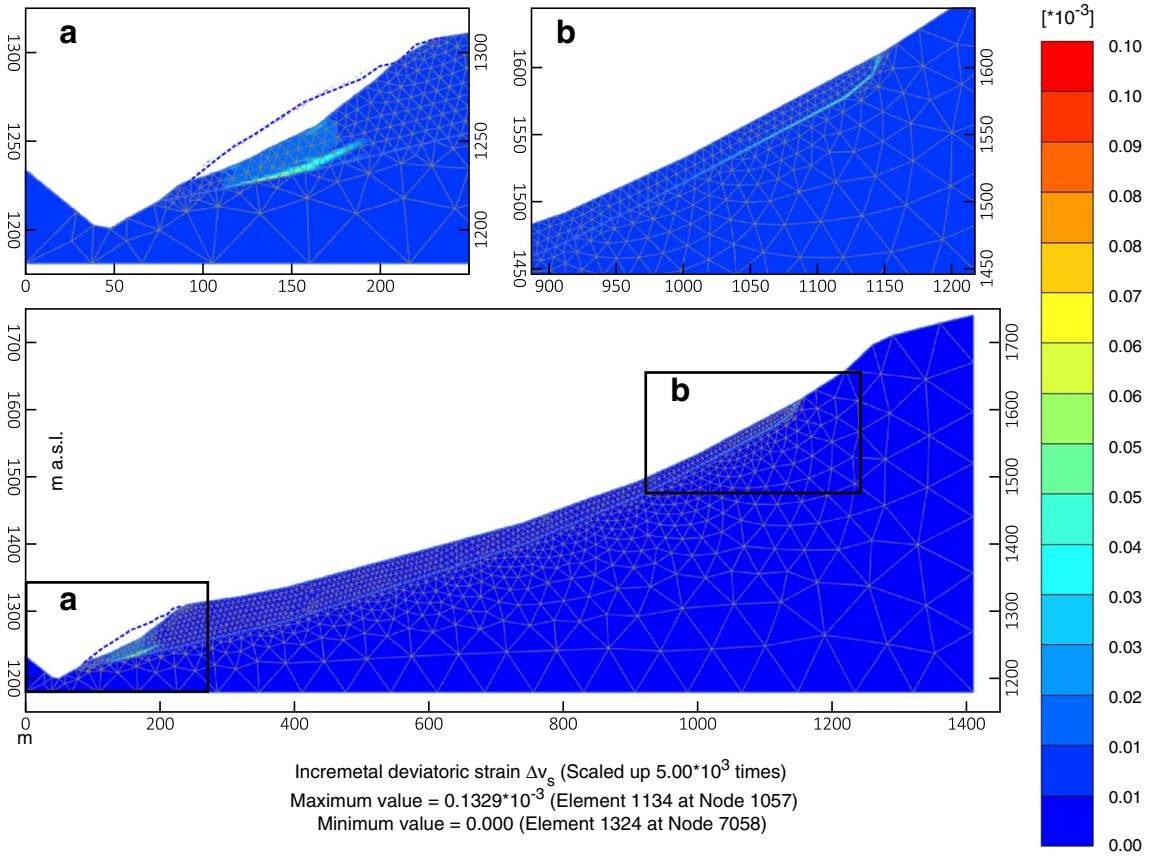

Fig. 16 Post-L1 landslide failure model; contours of the incremental deviatoric strain obtained for the critical GWL (25 m below ground level). **a** Detail of the incremental deviatoric strain at the bottom of the slope (rotational landslide L1). **b** Detail of the incremental deviatoric strain at the crown of landslide L2

Consequently, we can also expect an increase in the occurrence of sudden landslides. Landslides without monitoring systems and with a lack of ancillary data might be activated. Once such a landslide occurs, it is necessary to reconstruct its evolution and define its kinematics and triggering factors, as its eventual further activity may threaten human activity and life. The use of multidisciplinary and multidataset approaches is the best way to conduct a posteriori investigations of landslide behaviour. We used this approach to study the November 2016 Monesi di Mendatica landslide occurrence, as it represents all of the abovementioned problems. The results reveal several aspects worth discussing.

The studied landslide is characterized by rapid evolution during the extreme rainfall event and by low displacement rates before and after the event. To describe each evolution phase, which is represented by different velocity rates, we chose the most suitable technique. For the catastrophic phase, defined by a moderate displacement (up to 3–4 m) occurring within a few days, we applied the DIC technique. In the Monesi case, this technique detected subpixel displacement using Sentinel-2 data (10 m spatial resolution) with an acceptable precision, similar to that resulting from the higher resolution data of Planet. Considering the high frequency and cost-free nature of these data, it could be a valid methodology to map moderate landslide displacement. In contrast, to analyse pre- and post-catastrophic phases, which are defined by a velocity rate of a few millimetres per year, another approach, such as satellite SAR interferometry, should be used. Even though these techniques are suitable for different displacement magnitudes, their combined use can cover a large time interval and a significant range of displacement rates (from a few mm/year for SAR to several m/day for DIC).

The analysis of several monitoring datasets acquired after the main L2 reactivation, combined with InSAR data, allowed us to define the role of groundwater and rainfall in the evolution of the slope. We compared the postevent displacement detected by InSAR and GNSS with the 5-day cumulative rainfall and groundwater level. We observed a slight acceleration after the rainy periods (e.g. winter 2017–2018 and 2018–2019, e1 and e2 in Fig. 18a), when the groundwater level was notably high, and low velocity values during the dry periods (e.g. summer 2017 and 2019, d1 and d2 in Fig. 18 a and b). This limited landslide movement hampers a clear definition of its response time to groundwater level fluctuation, as was possible for the other landslides (e.g. Lollino et al. 2006). For short temporal spans, we could not detect acceleration correlated with rapid increases in groundwater due to the noise of the InSAR data. However, smoothing the data over a long time interval made it possible to empirically correlate the landslide velocity and the groundwater level (Fig. 18c). We noted that the velocity was several times higher during high water level periods than during droughts.

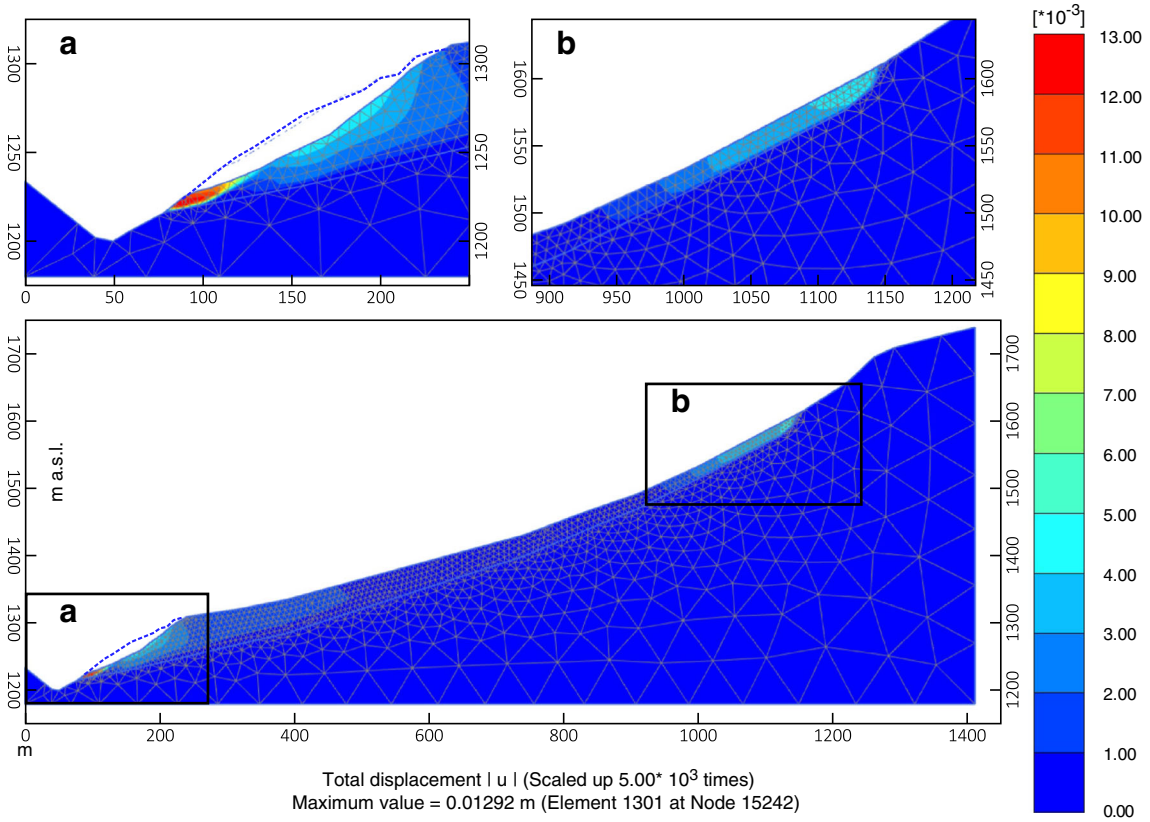

Fig. 17 Post-L1 landslide failure model; contours of the accumulated displacement obtained for the critical GWL (25 m below ground level). **a** Detail of the accumulated displacement at the bottom of the slope (rotational landslide L1). **b** Detail of the accumulated displacement at the main scarp of L2

Despite the limits related to the poor geotechnical and hydraulic characterization of the study area (in situ and laboratory testing), the numerical model provided good results. These results are not intended to be strictly quantitative; however, they provide a clear interpretation of mechanical slope behaviours, as represented by the failure mechanisms developed during landslide events, which supported the definition of landslide behaviour during the 2016 event. The numerical results showed the activation of the L1 landslide and the effect of its failure on the stability of the L2 landslide, as well as the importance of the groundwater table in the activation of these landslides. According to these results, slope management and remedial measures should carefully consider groundwater level management.

During the 2016 flood event, Bandita Creek, which flows along the landslide body, significantly increased its usual water supply to the basin and likely augmented the groundwater table within the highly permeable landslide body.

Conclusion

In this paper, we presented a reconstruction of a series of landslide events that occurred after extreme rainfall in November 2016 in the village of Monesi di Mendatica in the Ligurian Alps. We identified two landslide phenomena, i.e. the reactivation of a massive and deep-seated planar landslide (L2) and the activation of a rotational landslide (L1) located at the toe in the frontal part of the slope. To analyse these events, we used a multidisciplinary approach to define their sequence of appearances, kinematics, failure mechanisms and triggering factors. To achieve these goals, we collected various datasets and information sources (e.g. remote sensing data, rainfall records, geomorphological elements, subsurface investigation and postevent monitoring data, field survey observations) and applied several processing techniques. In the final step, we merged the obtained results, which allowed us to obtain a complete reconstruction to interpret the characteristics of the failure event and define its kinematics.

By analysing rainfall records, we found that the rainfall event (which dropped up to 700 mm in 5–6 days) that triggered the landslides was the most severe of the last seven decades (and probably on a century scale) in this area of the Ligurian Alps. Considering the Monesi di Mendatica slope, we did not find any records of any resulting antecedent landslide massive reactivations within at least the last 70 years.

We defined the sequence of events that occurred during the 2016 flood based on field observations, rainfall data and numerical modelling. This showed that most of the L2 displacement occurred within a few days after the rainfall event.

Regarding the landslide evolution, we obtained coevent displacement by applying the DIC technique to the images of two satellite sensors (Sentinel-2 and Planet). We estimated that the displacement of the whole landslide mass ranged from 2 to 4 m

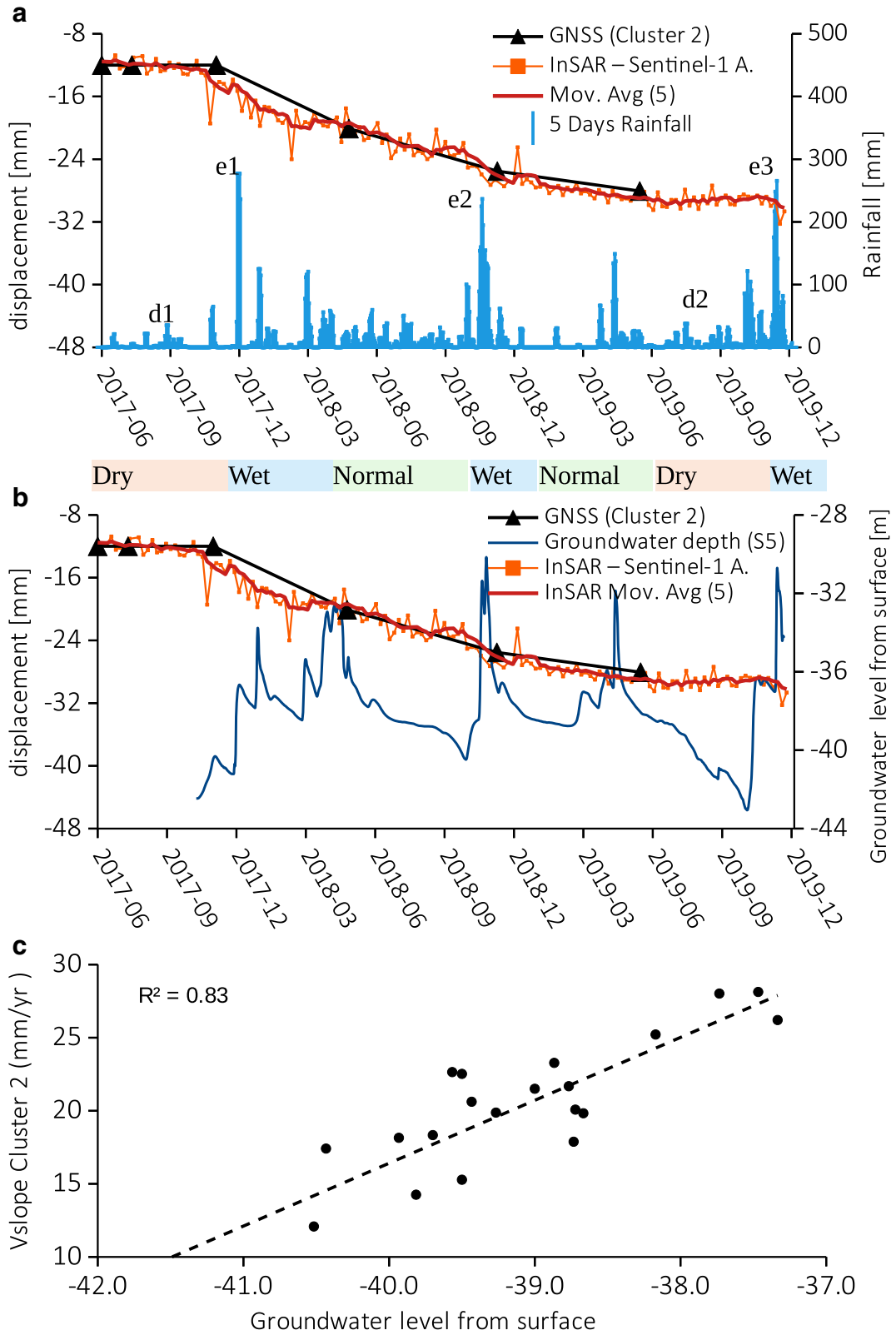

Fig. 18 Postevent InSAR and GNSS time series compared with **a** 5-day rainfall; **b** groundwater level in piezometer S5 (the events that caused slight acceleration are reported as e1, e2 and e3, while drought periods with low velocity are d1 and d2); and **c** scatter plot of the 6-month averaged VSLOPE (y-axis) over the 3-month averaged groundwater level (x-axis)

NNW. We used high-resolution aerial photographs to map landslide boundaries and visually validate the DIC results. Concerning the pre-catastrophic phase, we defined the corresponding displacement rate by analysing the InSAR data from the Sentinel-1 and Radarsat satellites. The results from both satellites indicate a slow landslide velocity (V_{SLOPE} up to 5 mm/year).

We also defined the postevent landslide kinematics based on ground-based and Sentinel-1 InSAR monitoring data (from 2017 to 2019). These measurements showed higher velocities (up to 25 mm/year) with respect to the pre-event period (2003-2016) located mainly in the NE sector of L2. This may suggest a change in landslide kinematics, but a more extended period of monitoring would be necessary to confirm such a trend. Additionally, the postevent time series, together with the corresponding piezometric and rainfall measurements, show that landslides respond to increases in groundwater level caused by intense rainfall or rapid snow melting. This agrees with the rapid evolution of the groundwater level resulting from the medium-high permeability of the landslide body (8.1 m/day).

We performed numerical modelling of the slope using the finite element approach. Even if the presented model represents a rough approximation of the mechanical and hydraulic behaviour, the numerical results appear to be realistic, as they show strain and displacement concentrations at the toe and crown of the landslide. These results are qualitatively coherent with the field observations and DIC results, and they support the definition of mechanisms and conditions leading to slope failure during the 2016 event. Finally, numerical results and postevent piezometric data allowed us to determine that the main trigger of the L1 and L2 phenomena was the significant increase in groundwater level (up to 12–15 m above average).

This multidisciplinary approach consists of utilizing various types of data and processing techniques. Each technique reveals a single landslide aspect to be later merged and interpreted as a unique dataset. This allowed for an almost complete understanding of landslide behaviour and a detailed landslide investigation. The key point of this approach is that it does not need a large amount of ancillary data for each method because their union compensates for the lack of information and in situ monitoring data. This approach is suitable to study poorly studied landslides with unexpected and abrupt reactivation events.

Acknowledgements

We would like to thank Dr. Flavio Poggi (Regione Liguria) for his effort and support in the coordination between municipalities, CNR and private consultants that participated in the study of the Monesi landslide and Dr. Macciò, who planned and managed the site investigations, drilling campaigns and in situ monitoring activities.

References

Agliardi F, Scuderi MM, Fusi N, Collettini C (2020) Slow-to-fast transition of giant creeping rockslides modulated by undrained loading in basal shear zones. Nature communications 11:1–11

Amanti M, Chiessi V, Guarino PM, et al (2016) Back-analysis of a large earth-slide in stiff clays induced by intense rainfalls

ARPA Piemonte (2017) Dataset su griglia NWIOI. https://www.arpa.piemonte.it/rischinaturali/tematismi/clima/confronti-storici/dati/dati.html#2.0. Accessed 13 Jan 2020

ARPA Piemonte, Regione Piemonte (2018) Gli eventi alluvionali in Piemonte - Evento del 21-25 novembre 2016. arpa.piemonte.it/news/evento-alluvionale-21-25-novembre-2016-la-pubblicazione. Accessed 25 May 2019

Avanzi GD, Galanti Y, Giannecchini R, Bartelletti C (2015) Shallow landslides triggered by the 25 October 2011 extreme rainfall in Eastern Liguria (Italy). In: Engineering Geology for Society and Territory-Volume 2. Springer, Berlin, pp 515–519

Baroň I, Ř ehánek T, Vošmik J, Musel V, Kondrová L (2011) Report on a recent deep-seated landslide at Gírová Mt., Czech Republic, triggered by a heavy rainfall: the Gírová Mt., Outer West Carpathians; Czech Republic. Landslides 8:355–361

Béjar-Pizarro M, Notti D, Mateos RM, Ezquerro P, Centolanza G, Herrera G, Bru G, Sanabria M, Solari L, Duro J, Fernández J (2017) Mapping vulnerable urban areas affected by slow-moving landslides using Sentinel-1 InSAR data. Remote Sensing 9:876

Berti M, Bertello L, Bernardi AR, Caputo G (2017) Back analysis of a large landslide in a flysch rock mass. Landslides 14:2041–2058

Bertolini G, Pizziolo M (2008) Risk assessment strategies for the reactivation of earth flows in the Northern Apennines (Italy). Engineering Geology 102:178–192

Bickel VT, Manconi A, Amann F (2018) Quantitative assessment of digital image correlation methods to detect and monitor surface displacements of large slope instabilities. Remote Sensing 10:865

Caporossi P, Mazzanti P, Bozzano F (2018) Digital image correlation (DIC) analysis of the 3 December 2013 Montescaglioso landslide (Basilicata, southern Italy): results from a multi-dataset investigation. ISPRS International Journal of Geo-Information 7:372

Casagli N, Cigna F, Bianchini S, Hölbling D, Füreder P, Righini G, del Conte S, Friedl B, Schneiderbauer S, Iasio C, Vlcko J, Greif V, Proske H, Granica K, Falco S, Lozzi S, Mora O, Arnaud A, Novali F, Bianchi M (2016) Landslide mapping and monitoring by using radar and optical remote sensing: examples from the EC-FP7 project SAFER. Remote sensing applications: society and environment 4:92–108

Cevasco A, Termini F, Valentino R, Meisina C, Bonì R, Bordoni M, Chella GP, de Vita P (2018) Residual mechanisms and kinematics of the relict Lemeglio coastal landslide (Liguria, northwestern Italy). Geomorphology 320:64–81

Cignetti M, Godone D, Giordan D (2019) Shallow landslide susceptibility, Rupinaro catchment, Liguria (northwestern Italy). Journal of Maps:1–13

Cooper AH (2008) The classification, recording, databasing and use of information about building damage caused by subsidence and landslides. Quarterly Journal of Engineering Geology and Hydrogeology 41:409–424

Crosta GB, Chen H, Lee CF (2004) Replay of the 1987 Val Pola landslide, Italian alps. Geomorphology 60:127–146

Crozier MJ (2010) Deciphering the effect of climate change on landslide activity: a review. Geomorphology 124:260–267

Dawson EM, Roth WH, Drescher A (1999) Slope stability analysis by strength reduction. Geotechnique 49(6):835–840. https://doi.org/10.1680/geot.1999.49.6.835

Debella-Gilo M, Kääb A (2011) Sub-pixel precision image matching for measuring surface displacements on mass movements using normalized cross-correlation. Remote Sensing of Environment 115:130–142

Dematteis N, Giordan D (2021) Comparison of digital image correlation methods and the impact of noise in geoscience applications. Remote Sensing 13:327. https://doi.org/10.3390/rs13020327

Dematteis N, Giordan D, Zucca F, Luzi G, Allasia P (2018) 4D surface kinematics monitoring through terrestrial radar interferometry and image cross-correlation coupling. ISPRS journal of photogrammetry and remote sensing 142:38–50

Dematteis N, Giordan D, Allasia P (2019) Image classification for automated image cross-correlation applications in the geosciences. Applied Sciences 9:2357

Federici PR, Chelli A, Biagioni F, Rapetti F (2007) Atlante dei centri abitati instabili della Liguria. Liguria, Regione

Ferretti A, Fumagalli A, Novali F, Prati C, Rocca F, Rucci A (2011) A new algorithm for processing interferometric data-stacks: SqueeSAR. IEEE transactions on geoscience and remote sensing 49:3460–3470

Fienup JR (1997) Invariant error metrics for image reconstruction. Applied optics 36:8352–8357

Frattini P, Crosta GB, Rossini M, Allievi J (2018) Activity and kinematic behaviour of deep-seated landslides from PS-InSAR displacement rate measurements. Landslides 15:1053–1070

Gallus WA Jr, Parodi A, Maugeri M (2018) Possible impacts of a changing climate on intense Ligurian Sea rainfall events. International Journal of Climatology 38:e323–e329

Gao L, Zhang LM, Cheung RWM (2018) Relationships between natural terrain landslide magnitudes and triggering rainfall based on a large landslide inventory in Hong Kong. Landslides 15:727–740

Gariano SL, Guzzetti F (2016) Landslides in a changing climate. Earth-Science Reviews 162:227–252
Giordan D, Cignetti M, Baldo M, Godone D (2017a) Relationship between man-made environment and slope stability: the case of 2014 rainfall events in the terraced landscape of the Liguria region (northwestern Italy). Geomatics, Natural Hazards and Risk 8:1833–1852
Giordan D, Cignetti M, Bertolo D (2017b) The use of morpho-structural domains for the characterization of deep-seated gravitational slope deformations in Valle d'Aosta. In: Workshop on World Landslide Forum. Springer, Berlin, pp 59–68
Giordan D, Notti D, Villa A, Zucca F, Calò F, Pepe A, Dutto F, Pari P, Baldo M, Allasia P (2018) Low cost, multiscale and multi-sensor application for flooded area mapping. Nat Hazards Earth Syst Sci 18(5):1493–1516
Giordan D, Dematteis N, Allasia P, Motta E (2020) Classification and kinematics of the Planpincieux Glacier break-offs using photographic time-lapse analysis. Journal of Glaciology 66:188–202
Guzzetti F, Cardinali M, Reichenbach P, Cipolla F, Sebastiani C, Galli M, Salvati P (2004) Landslides triggered by the 23 November 2000 rainfall event in the Imperia Province, Western Liguria, Italy. Engineering Geology 73:229–245
Guzzetti F, Peruccacci S, Rossi M, Stark CP (2007) Rainfall thresholds for the initiation of landslides in central and southern Europe. Meteorology and atmospheric physics 98:239–267
Guzzetti F, Peruccacci S, Rossi M, Stark CP (2008) The rainfall intensity–duration control of shallow landslides and debris flows: an update. Landslides 5:3–17
Handwerger AL, Huang M-H, Fielding EJ et al (2019) A shift from drought to extreme rainfall drives a stable landslide to catastrophic failure. Scientific reports 9:1–12
Hoek E, Brown ET (2019) The Hoek–Brown failure criterion and GSI – 2018 edition. J Rock Mech Geotech Eng 11(3):445–463. https://doi.org/10.1016/j.jrmge.2018.08.001
IPCC – Intergovernmental Panel on Climate Change (2014) Climate change 2014: synthesis report. Contribution of Working Groups I. II and III to the Fifth Assessment Report of the Intergovernmental Panel on Climate Change, Geneve
ISPRA (2012) Hydrological yearbooks. In: Hydrological yearbooks. http://www.isprambiente.gov.it/en/projects/inland-waters-and-marine-waters/hydrological-yearbooks?set_language=en. Accessed 13 Jan 2020
Iverson RM (2000) Landslide triggering by rain infiltration. Water resources research 36:1897–1910
Lanteaume M, Radulescu N, Gravos M, et al (1990) Notice explicative, Carte Géologique de France (1/50.000), feuille Vève-Tende (948). Bureau de Recherches Géologiques et Minières, Orléans
Leprince S, Barbot S, Ayoub F, Avouac J-P (2007) Automatic and precise orthorectification, coregistration, and subpixel correlation of satellite images, application to ground deformation measurements. IEEE Transactions on Geoscience and Remote Sensing 45:1529–1558
Lollino G, Arattano M, Allasia P, Giordan D (2006) Time response of a landslide to meteorological events
Lollino P, Giordan D, Allasia P (2014) The Montaguto earthflow: A back-analysis of the process of landslide propagation. Eng Geol 170:66–79. https://doi.org/10.1016/j.enggeo.2013.12.011
Lollino P, Cotecchia F, Elia G, Mitaritonna G, Santaloia F (2016) Interpretation of landslide mechanisms based on numerical modelling: two case-histories. European Journal of Environmental and Civil Engineering 20:1032–1053
Longoni L, Papini M, Brambilla D, Arosio D, Zanzi L (2016) The role of the spatial scale and data accuracy on deep-seated gravitational slope deformation modeling: the Ronco landslide, Italy. Geomorphology 253:74–82
Luino F (1999) The flood and landslide event of November 4–6 1994 in Piedmont Region (Northwestern Italy): causes and related effects in Tanaro Valley. Physics and Chemistry of the Earth, Part A: Solid Earth and Geodesy 24:123–129
Luzi G, Dematteis N (2019) Ku band terrestrial radar observations by means of circular polarized antennas. Remote Sensing 11:270
Maino M, Seno S (2016) The thrust zone of the Ligurian Penninic basal contact (Monte Fronté, Ligurian Alps, Italy). Journal of Maps 12:341–351
Manconi A, Kourkouli P, Caduff R, Strozzi T, Loew S (2018) Monitoring surface deformation over a failing rock slope with the ESA Sentinels: insights from Moosfluh instability, Swiss Alps. Remote Sensing 10:672
Mantovani M, Devoto S, Forte E, Mocnik A, Pasuto A, Piacentini D, Soldati M (2013) A multidisciplinary approach for rock spreading and block sliding investigation in the northwestern coast of Malta. Landslides 10:611–622
Marinos P, Hoek E (2000) GSI: a geologically friendly tool for rock mass strength estimation. In: ISRM international symposium. International Society for Rock Mechanics and Rock Engineering
Notti D, Herrera G, Bianchini S, Meisina C, García-Davalillo JC, Zucca F (2014) A methodology for improving landslide PSI data analysis. International Journal of Remote Sensing 35:2186–2214
Notti D, Giordan D, Caló F, Pepe A, Zucca F, Galve J (2018) Potential and limitations of open satellite data for flood mapping. Remote Sensing 10:1673
Park CB, Miller RD, Xia J (1999) Multichannel analysis of surface waves. Geophysics 64:800–808
Peduto D, Nicodemo G, Caraffa M, Gullà G (2018) Quantitative analysis of consequences to masonry buildings interacting with slow-moving landslide mechanisms: a case study. Landslides 15:2017–2030
Pepe G, Piazza M, Cevasco A (2015) Geomechanical characterization of a highly heterogeneous flysch rock mass by means of the GSI method. Bulletin of Engineering Geology and the Environment 74:465–477
Pepe G, Mandarino A, Raso E, et al (2019) Extreme flood and landslides triggered in the Arroscia Valley (Liguria Region, Northwestern Italy) during the November 2016 rainfall event. In: IAEG/AEG Annual Meeting Proceedings, San Francisco, California, 2018-Volume 1. Springer, pp 171–175
Peruccacci S, Brunetti MT, Gariano SL, Melillo M, Rossi M, Guzzetti F (2017) Rainfall thresholds for possible landslide occurrence in Italy. Geomorphology 290:39–57
Petkovšek A, Kočevar M, Maček M et al (2011) The Stogovce landslide in SW Slovenia triggered during the September 2010 extreme rainfall event. Landslides 8:499–506
PLAXIS 2D (2019) PLAXIS 2D CONNECT Edition V20 - Reference manual. Delft, Netherlands
Ramasco M, Troisi C (2002) Grandi fenomeni franosi attivatisi a seguito dell'evento dell'ottobre 2000 in: Eventi alluvionali in Piemonte: 10-14 giugno 2000. ARPA Piemonte, Turin
Scambos TA, Dutkiewicz MJ, Wilson JC, Bindschadler RA (1992) Application of image cross-correlation to the measurement of glacier velocity using satellite image data. Remote sensing of environment 42:177–186
Stoffel M, Tiranti D, Huggel C (2014) Climate change impacts on mass movements—case studies from the European Alps. Science of the Total Environment 493:1255–1266
Stumpf A, Malet J-P, Delacourt C (2017) Correlation of satellite image time-series for the detection and monitoring of slow-moving landslides. Remote sensing of environment 189:40–55
Tiranti D, Rabuffetti D (2010) Estimation of rainfall thresholds triggering shallow landslides for an operational warning system implementation. Landslides 7:471–481
Tomás R, Abellán A, Cano M, Riquelme A, Tenza-Abril AJ, Baeza-Brotons F, Saval JM, Jaboyedoff M (2018) A multidisciplinary approach for the investigation of a rock spreading on an urban slope. Landslides 15:199–217
Trigila A, Iadanza C, Spizzichino D (2008) IFFI Project (Italian landslide inventory) and risk assessment. In: Proceedings of the First World Landslide Forum. Springer-Verlag, Berlin Heidelberg, pp 18–21
Turco M, Zollo AL, Ronchi C et al (2013) Assessing gridded observations for daily precipitation extremes in the Alps with a focus on northwest Italy. Natural Hazards & Earth System Sciences:13
Vanossi M, Cortesogno M, Galbiati B et al (1984) Geologia delle Alpi Liguri: dati, problemi, ipotesi. Memorie della Societa Geologica Italiana 28:5–75
Zêzere JL, Trigo RM, Trigo IF (2005) Shallow and deep landslides induced by rainfall in the Lisbon region (Portugal): assessment of relationships with the North Atlantic Oscillation. Natural Hazards and Earth System Science 5:331–344

Supplementary Information The online version contains supplementary material available at https://doi.org/10.1007/s10346-021-01651-3.

D. Notti · A. Wrzesniak (✉) · N. Dematteis · D. Giordan
National Research Council of Italy, Research Institute for Geo-Hydrological Protection (CNR-IRPI),
Strada delle Cacce 73, 10135, Torino, Italy
Email: aleksandra.wrzesniak@irpi.cnr.it

P. Lollino · N. L. Fazio
National Research Council of Italy, Research Institute for Geo-Hydrological Protection (CNR-IRPI),
Via Amendola, 122, 70126, Bari, Italy

F. Zucca
Department of Earth and Environmental Science,
University of Pavia,
Via Ferrata 1, 27100, Pavia, Italy